Table 1
Summary of rat cardiac grafting

Groups# (n)	Donor→recipient	Graft survival (days)	MST
1a(6)	DA→DA	>100×6	100
1b(5)	DA→EGFP-DA	>100×5	100
1c(8)	EGFP-DA→EGFP-DA	>100×8	100
1d(8)	EGFP-DA→DA	35, 78, >100×6	100
2a(8)	EGFP-DA→DA with lenti-DC	9, 12, 13×3, 14, 17, 25	13
2b(7)	EGFP-DA→DA with lenti-PEM	15, 22, 23, ×2, 24, 25, 29	23
3a(6)	EGFP-DA→DA with lenti-mDC	36, >100×5	100
3b(10)	EGFP-DA→DA with adeno-mDC	47, 65, >100×8	100
3c(7)	EGFP-DA→DA with adeno-PEM	11×3, 12, 15, 17, 22	12

#1a: From non-transgenic male DA littermate donors to normal male DA recipients.
1b: From non-transgenic male DA littermate donors to EGFP transgenic male DA recipients.
1c: From EGFP transgenic male DA littermate donors into EGFP transgenic male DA recipients.
1d: From EGFP-transgenic male DA littermate donors into normal male DA recipients.
2a: Normal DA recipients rats that had been immunized with 2×10^5 EGFP-transduced DC by lentiviral vector (lenti-DC, see also Figs. 5, 6 and 7B), was subsequently isografted with EGFP transgenic male DA donor hearts.
2b: Normal DA recipients rats that had been immunized with 2×10^5 EGFP-transduced PEM by lentiviral vector (lenti-PEM, see also Fig. 8), was subsequently isografted with EGFP transgenic male DA donor hearts.
3a: Normal DA recipients rats that had been pre-immunized with 2×10^5 EGFP-transduced DC, was subsequently isografted with EGFP transgenic male DA donor hearts. The DC generated from a long-term culture had been purified with CD161a (mature DC) and then treated by EGFP-lentiviral vector at 5 MOI for seven days (lenti-mDC, see also Fig. 7A).
3b: Normal DA recipients rats that had been pre-immunized with 2×10^5 EGFP-transduced DC, were subsequently isografted with EGFP transgenic male DA donor hearts. The DC generated from a long-term culture had been purified with CD161a (mature DC) and then treated by EGFP-adenoviral vector at 100 MOI for five days (adeno-mDC, see also Fig. 4).
3c: Normal DA recipients rats that had been pre-immunized with 2×10^5 EGFP-transduced PEM, were subsequently isografted with EGFP transgenic male DA donor hearts. The CD3−CD4+ PEM purified from PEC were treated by EGFP-adenoviral vector at 100 MOI for five days (adeno-PEM, see also Fig. 3A).

EGFP) established and described by Dr. Okabe and his group [28] was generously provided to us and further backcrossed into DA background for more than eight generations and maintained in our Institute. During the backcross, it was established that EGFP transgenic and/or non-transgenic littermates accepted parental EGFP transgenic and DA skin isografts respectively. Animals were maintained in our animal facility under specific pathogen free conditions.

3.2. Cardiac transplantation

Heterotopic auxiliary cardiac grafting was performed into the abdominal cavity of recipients by the classical methods reported by Ono and Lindsey [29]. Combinations between donor cardiac grafts and recipients were formed using male rats, and grafts were inspected and palpated daily after grafting. The completion of cardiac graft rejection was defined by the cessation of graft palpitation and was routinely confirmed by histological findings, i.e., admixtures of moderate to severe cardiac myocytes necrosis accompanied by perivascular mononuclear cell infiltration in the graft sections with hematoxylin and eosin-staining. It should be mentioned that an apparent technical error that resulted in cardiac arrest judged by palpation within three days was excluded from the group.

3.3. Sensitization of non-transgenic littermate to EGFP transduced APC

DC or PEM prepared under the several conditions as described below by either culturing BMC with cytokine combinations of human Flt3/Flk2 (fms-like tyrosine kinase-3/fetal liver kinase-2) ligand and human IL-6 (Interleukin-6) or freshly isolated PEM and cells that had been subjected to EGFP transduction were resuspended in cold Dulbecco's phosphate-buffered saline (D-PBS) at a concentration of 1×10^6/ml. The cells were inoculated into each recipient's hind footpad (0.1 ml of 1×10^5 cells×2/rat).

3.4. Experiment groups

Cardiac transplantation was performed in the following experiment groups (Table 1):

Group 1 consisted of primary cardiac isograftings and they are as follows.

1a: From non-transgenic male DA littermate donors to normal male DA recipients
1b: From non-transgenic male DA littermate donors to EGFP transgenic male DA recipients
1c: From EGFP transgenic male DA littermate donors to EGFP transgenic male DA recipients
1d: From EGFP-transgenic male DA littermate donors to normal male DA recipients

Group 2 consisted of secondary cardiac isografting following EGFP-transduced APC challenge and they are as follows.

2a: Normal DA recipients that had been immunized with 2×10^5 EGFP-transduced DC by total four MOI of lentiviral vector (*lenti-DC*) two

Table 2
Summary of a correlation between gene transduction efficiency and the sensitization effect on cardiac isografts

Gene transduction				Transplantation	
Vector[a]	Target cells[a]	(cells of sensitivation)[b]	%EGFP+[c]	Cardiac Tx[d]	Days (MST[e])
Adeno-EGFP	DC-enrich	(adeno-DC in Fig. 3B)	16%	(−)[f]	(−)[f]
	CD161a DC	(adeno-mDC in Fig. 4)	2.3%	Group 3b	100
	PEM	(adeno-PEM in Fig. 3A)	74%	Group 3c	12
Lenti-EGFP	DC-enrich	(lenti-DC in Fig. 7B)	91%	Group 2a	13
	CD161a DC	(lenti-mDC in Fig. 7A)	0.4%	Group 3a	100
	PEM	(lenti-PEM in Fig. 8)	7.5%	Group 2b	23

[a] See Materials and methods.
[b] EGFP-transduced cells for sensitization are shown in each figure.
[c] EGFP expression of transduced cells was analyzed by flowcytometry.
[d] Groups of heterotopic cardiac isografting.
[e] Isograft Survival (Days of median survival time) were analyzed by Kaplan–Meier's method (log rank test). 2a vs 2b: $p=0.029$, 2b vs 3c: $p=0.002$, 2a vs 3c: $p=0.68$ (not significant).
[f] Not tested.

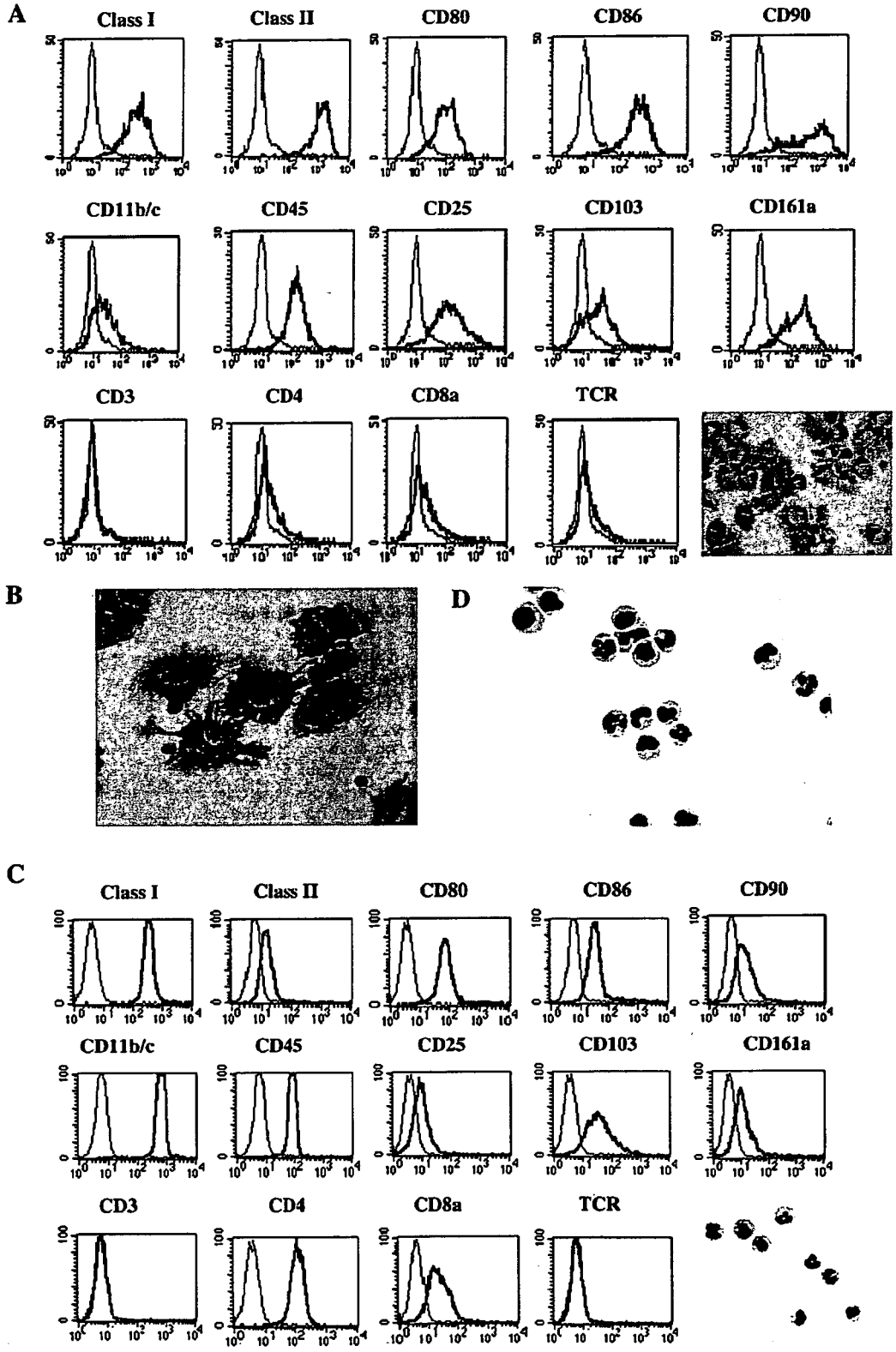
A
Class I
Class II
CD80
CD86
CD90
CD11b/c
CD45
CD25
CD103
CD161a
CD3
CD4
CD8a
TCR
B
D
C
Class I
Class II
CD80
CD86
CD90
CD11b/c
CD45
CD25
CD103
CD161a
CD3
CD4
CD8a
TCR

weeks before were subsequently isografted with EGFP transgenic male DA donor hearts.
Representative figure demonstrating the efficiency of EGFP induction in DC is shown in Figs. 5, 6 and 7B.

2b: Normal DA recipients that had been immunized with 2×10^5 EGFP-transduced PEM by five MOI of lentiviral vector (*lenti-PEM*) two weeks before were subsequently isografted with EGFP transgenic male DA donor hearts.
The efficiency of EGFP induction in PEM is shown in Fig. 8.

Likewise, Group 3 consisted of secondary cardiac isografting following APC challenge and they are as follows.

3a: Normal DA recipients that had been pre-immunized with 2×10^5 EGFP-transduced DC were subsequently isografted with EGFP transgenic male DA donor hearts.
The DC generated from a long-term culture were first purified with CD161a (*mature DC: mDC*) and then treated by EGFP-lentiviral vector at five MOI for seven days (*lenti-mDC*).
The efficiency of EGFP-transduction in mature DC is shown in Fig. 7A.

3b: Normal DA recipients that had been pre-immunized with 2×10^5 EGFP-transduced DC were subsequently isografted with EGFP transgenic male DA donor hearts.
The DC generated from a long-term culture were purified with CD161a (mature DC) and then treated by EGFP-adenoviral vector at 100 MOI for five days (*adeno-mDC*).
The relative efficiency of EGFP-transduction in mature DC is shown in Fig. 4.

3c: Normal DA recipients that had been pre-immunized with 2×10^5 EGFP-transduced PEM two weeks before were subsequently isografted with EGFP transgenic male DA donor hearts.
The CD3−CD4+ PEM purified from PEC were treated by EGFP-adenoviral vector at 100 MOI for five days (*adeno-PEM*).
The representative efficiency of EGFP-transduction in PEM is shown in Fig. 3A.

3.5. Statistical analysis

Statistical analysis was performed using Kaplan–Meier's method (Fig. 2). A p value <0.05 was considered significant by a log rank test (Table 2).

3.6. Reagents

Monoclonal antibodies (mAbs) that included mouse anti-rat PE-CD4, PE-CD8, PE-class II (OX-6), PE-CD80, PE-CD86, PE-CD161a (NKR-P1A, 3.2.3), Biotinated-CD161a, FITC-class I (OX-18), FITC-class II (OX-6), FITC-CD80, FITC-CD86, FITC-CD11b/c, FITC-CD45, FITC-CD25, FITC-CD103 (OX-62), FITC-CD161a, FITC-CD90, FITC-CD3, FITC-CD4, FITC-CD8a, and FITC-TCR were purchased from BD Immunocytometry products (BD Pharmingen International, Fujisawa Pharmaceutical Co., Ltd., Osaka, Japan). Cytokines that included recombinant human IL-6 (Interleukin-6) were generously supplied by Kirin Brewer Company Ltd., (Maebashi, Gunma, Japan). Recombinant human Flt3/Flk2 (fms-like tyrosine kinase-3/fetal liver kinase-2) ligand was purchased from PeproTech, Inc. USA (IBL Co., Ltd., Gunma, Japan).

3.7. Culture medium

The medium for primary cell preparation was Dulbecco's phosphate-buffered saline (D-PBS) (DAB, OXOID Ltd., Basingstoke, Hampshire, United Kingdom). For cell cultures, GIT (NIHON Pharmaceutical Co., Ltd. Tokyo, Japan) supplemented with 2 mmol/L L-glutamine and antibiotics without 2-mercaptoethanol was employed for long-term culture of rat BMC.

3.8. DC generation by a long-term BMC culture

Femurs and tibias were removed from rats, and BMC were obtained by flushing each bone cavity with 4 ml D-PBS. The cells were centrifuged once and resuspended, then filtered by 70 μl nylon mesh (BD Falcon™ Cell Strainer, BD Bioscience, USA). The cells were centrifuged again and resuspended, then centrifuged with Ficoll-Paque™ PLUS (d: 1.077, Amersham Bioscience, Uppsala, Sweden) at 2600 rpm for 25 min at 4 °C. Following density gradient centrifugation, the low-density cell fraction was harvested, centrifuged and resuspended and then washed twice with GIT medium. We previously reported that the low-density fraction (d; 1.077) prepared by density gradient centrifugation in lymphocyte separation medium (Ficoll-Paque™ PLUS) was a major source of bone marrow derived DC, not the high-density fraction (d; 1.094) [25]. The cells were cultured in 25 cm^2 cell culture flasks (Coster, Corning Incorporated, NY, USA) with recombinant human Flt3/Flk2 ligand (100 ng/ml) and IL-6 (10 ng/ml). Every five to six days, free-floating cells were harvested and re-cultured with fresh medium supplemented with the cytokines. The DC-enriched cell population was harvested as free-floating cells on day 21 during a long-term BMC culture of DA rat. This cell fraction contains 40–60% of DC (admixture of macrophages, DC progenitors and mature DC). The DC driven by Flt3/Flk2 ligand are currently classified as plasmacytoid DC that are distinguished from GM-CSF-dependent myeloid DC.

3.9. DC separation by AutoMACS system

The positive and/or negative selection of cells was performed according to the manufacturer's procedures (AutoMACS systems: Miltenyi Biotec, Bergisch Gladbach, Germany), Briefly, cells were first incubated with FcR-blocking antibody for 10 min on ice and then stained with either PE- or biotinated monoclonal antibody for 30 min on ice. After washing twice with D-PBS, the cells were further incubated with anti-PE or anti-biotin magnetic microbeads (10^7 cells/20 μl) Miltenyi Biotec, Bergisch Gladbach, Germany), and incubated for 30 min at 4 °C . Cells bound by magnetic-beads were likewise washed carefully and resuspended in 4 ml buffer solution, followed by magnetic separation by an AutoMACS system. The rat DC-enriched cell population was labeled with either Biotinated-anti-NKR-P1A (Natural Killer Receptor-Protein 1A) mAb or PE-anti-NKR-P1A mAb, and hence with anti-biotin microbeads or anti-PE microbeads, respectively. The cells were selected positively by an AutoMACS (Magnetic Cell Sorting) apparatus. These selected DC were homogeneous and more than 95% CD161a positive [25]. They were fully matured phenotypes (Fig. 1A and B).

3.10. Peritoneal exudate cells (PEC) and separation of peritoneal exudate macrophages (PEM)

Peritoneal exudate cells (PEC) [30] were obtained by flushing the peritoneal cavity with 50 ml D-PBS. The cells were centrifuged once, resuspended, and then filtered by a 70 μl nylon mesh (BD Falcon™ Cell Strainer, BD Bioscience, USA). The cells were centrifuged again, resuspended, and then centrifuged with Ficoll-Paque™ PLUS (d: 1.077, Amersham Bioscience, Uppsala, Sweden) at 2600 rpm for 25 min at 4 °C. Following density gradient centrifugation, the low-density cell fraction was harvested, centrifuged, resuspended, and washed twice with GIT medium.

The PEC were firstly subjected to negative selection by PE-anti-CD3 antibody with anti-PE microbeads, and the CD3 negative PEC were subsequently purified by FITC-anti-CD4 with anti-FITC microbeads as described above.

Fig. 1. (A) Phenotypic analysis of rat DC. These DC were generated from a long-term culture of BMC driven by Flt3/Flk2 ligand and IL-6 described in Materials and methods. Cells obtained from three weeks' culturing were analyzed by FITC- or PE-conjugated monoclonal antibodies. (B) Morphologic feature of rat DC. Cytospin of veiled form of DC was stained by May–Gruenwald and Giemsa methods. Flow cytometric analysis of these cells is shown in (A). (C) Phenotypic analysis of rat PEM. These PEM were separated from peritoneal exudate cells by AutoMACS systems described in Materials and methods. Cells were negatively depleted of CD3+ cells, and then CD4+ cells were further positively selected and analyzed by flow cytometry. (D) Morphologic feature of rat PEM. Cytospin of CD3−CD4+ peritoneal macrophages (PEM) was stained by May–Gruenwald and Giemsa methods. Flow cytometric analysis of these cells is shown in (C).

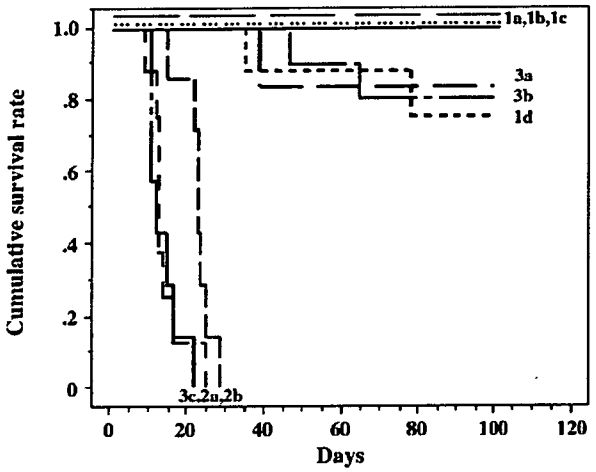

Fig. 2. Survival curves of cardiac isografts shown by Kaplan–Meier's method. EGFP-transduced DC and PEM were found to effectively induce EGFP-transgenic cardiac isograft rejection, although the former was significantly more effective than the latter (Group2a versus Group2b, $p=0.029$, by log rank test). Groups 1 (1a to 1d) consisted of primary cardiac isografting. 1a: From non-transgenic male DA littermate donors to normal male DA recipients. 1b: From non-transgenic male DA littermate donors to EGFP transgenic male DA recipients. 1c: From EGFP-transgenic male DA littermate donors to EGFP transgenic male DA recipients. 1d: From EGFP-transgenic male DA littermate donors to normal male DA recipients. Group 2 (2a to 2b) consisted of secondary cardiac isografting from EGFP-transgenic donor hearts. Normal DA recipients primed with EGFP transduced DC (Group 2a: lenti-DC in Figs. 7B, 5 and 6)) or EGFP transduced PEM (Group2b: lenti-PEM in Fig. 8) by lentiviral vectors were subsequently grafted with the EGFP-transgenic cardiac isografts. Group 3 (3a to 3c) was likewise from secondary cardiac isografting. Normal DA recipients were primed with either CD161a+ DC that had been treated with EGFP-lentiviral (Group 3a: lenti-mDC in Fig. 7A) and EGFP-adenoviral (Group 3b: adeno-mDC in Fig. 4) vectors. Likewise normal DA recipients primed with PEM treated by EGFP-adenoviral (Group 3c: adeno-PEM in Fig. 3A) vectors were subsequently grafted with EGFP-transgenic cardiac isografts.

These CD3−CD4+ macrophages were used as Peritoneal Exudate Macrophages (PEM).

The phenotype of PEM and its typical cytospin figure are presented in Fig. 1C and D, respectively.

3.11. Vector systems

Two viral vector systems were employed in order to transduce the EGFP gene into rat DC and PEM.

1) Adenoviral vector (Adeno-EGFP): titer 1×10^9 pfu/ml
2) Lentiviral vector (Lenti-EGFP): titer 1.27×10^9 pfu/ml

3.12. Recombinant adenoviral vector containing EGFP gene (Adeno-EGFP)

The recombinant adenovirus Ax1CAegfp, which contained an enhanced green fluorescent protein (EGFP) gene, was purchased from Riken Biosource Center, Tsukuba, JAPAN. This adenoviral vector was a replication-incompetent, E1- and E3-deficient recombinant adenovirus type 5 (Ad5) [31].

3.13. Adenoviral transduction of rat DC-enriched cell population, CD161a+ mature DC and PEM

Transduction of cells by adenoviral vectors was performed at a multiplicity of infection (MOI) value of 100 for 24 h at 37 °C in a 5% CO_2 incubator. Target cells, including rat DC-enriched cell populations (*adeno-DC* in Fig. 3B), purified CD161a+ mature DC (adeno-mDC in Fig. 4), and PEM (adeno-PEM in Fig. 3A), were washed once in culture medium and then culture was continued. FACS analysis was performed 2 days later.

3.14. Preparation of HIV-based lentiviral vector containing EGFP gene (Lenti-EGFP)

The HIV vectors were produced by co-transfecting 293FT cells with pHIV-CS-CDF-CG (cPPT-containing SIN vector plasmid encoding EGFP under control of CMV promoter, woodchuck hepatitis virus posttranslational regulatory element (WPRE) was ligated at the 3′-end of EGFP), pMDLg/p RRE (encoding packaging protein), pMD.G (encoding VSV-G envelop protein), and pRSV-Rev by calcium phosphate transfection as previously described [27]. The virus-containing supernatant was collected, passed through a 0.45 μm filter, and concentrated by centrifugation at 19.4 K at 21 °C for 2 h. The viral pellet was resuspended, concentrated again, frozen and stored at −80 °C. Vector preparations were titrated by infecting 293FT cells. The titer of the concentrated vector used in this study was about 1×10^9 pfu/mL.

3.15. Lentiviral transduction of rat BMC, DC-enriched cell population, CD161a+ mature DC, and PEM

Based on our previous studies [20], four types of transduction protocols were attempted, and the most efficient protocol for EGFP transduction into developing DC progenitors was determined. It is very important to employ developing DC progenitors for efficient gene transduction. Thus fresh rat BMC were cultured without EGFP-lentiviral vector for the first week. Thereafter, EGFP-lentiviral vector was added once a week for two successive weeks (lenti-DC in Fig. 7B). On day 21, CD161a and EGFP positive DC (1×10^5 cells/0.1 ml×2) were employed for in vivo priming.

Rat DC-enriched cell populations generated without the lentiviral vector were harvested on day 21, labeled with PE-NKRP1A mAb and anti-PE microbeads, and separated positively by an AutoMACS system. CD161a+ DC were collected as a homogeneous mature DC-population and admixed with five MOI of EGFP-lentiviral vector. Flowcytometric assay was performed 7 days later (lenti-mDC in Fig. 7A). When PEM were targeted with EGFP-lentiviral vector systems, five MOI for two weeks' treatment was employed (lenti-PEM in Fig. 8).

3.16. Flow cytometric analysis

The harvested cell suspension was stained with monoclonal antibodies and analyzed by flow cytometry using a FACScan (Becton Dickinson Immunocytometry Systems, San Jose, CA). Briefly, DC-enriched cells or CD161a+ DC were centrifuged once and then resuspended in D-PBS. The cells were incubated with FcR-blocking antibody for 10 min on ice and then stained with PE-conjugated monoclonal antibody for 30 min on ice. After washing twice with D-PBS, the cells were carefully resuspended in 1.5 ml D-PBS. Flow cytometry was performed on a FACScan and the data were analyzed with CELLQuest software (Becton Dickinson). We collected 10,000 events per sample. Gating of the cells was determined with the use of appropriate isotype controls. Results are given as the percentage positive minus backgrounds from appropriate isotype controls.

3.17. Cytologic analysis

To assess the morphological features of rat DC, PEM and the EGFP expression of gene-transduced DC and PEM, cytospin preparations of 1×10^4 harvested cells were made in a cytocentrifuge (Shandon, Pittsburgh, Pa. USA) at 800 rpm for 10 min, stained with May–Gruenwald and Giemsa (Merck Japan, Tokyo, Japan), and examined by light microscopy and fluoroscopy. Phase-contrast and fluoroscopic observation of cultures was made by inverted microscopy (OPLYMPUS, Tokyo, Japan).

4. Results

DC and PEM employed in this studies were established to be professional APC for T-cell activation and cytotoxic T-cell induction

[32]. We previously fully described phenotypes and functions of rat DC generated by a long-term culture method with cytokine combinations of human Flt3/Flk2 ligand and human IL-6 employing a low-density fraction (d: 1.077) of rat BMC [25].

The DC driven by Flt3/Flk2 ligand are currently considered and classified as plasmacytoid DC (pDC) based on the cytokine profiles as well as differential expression of toll-like receptors (TLR).

To compare the phenotypic differences between BMC-derived DC and PEM, we re-examined the phenotypes of PEM and compared them to those of DC harvested from BMC culture on day 21. Fig. 1A and B display the results for DC driven by Flt3/Flk2 ligand and IL-6. Likewise Fig. 1C and D displays results for PEM. Flowcytometric analysis revealed that fully mature DC generated by cytokine combinations of human Flt3/Flk2 ligand and human IL-6 expressed

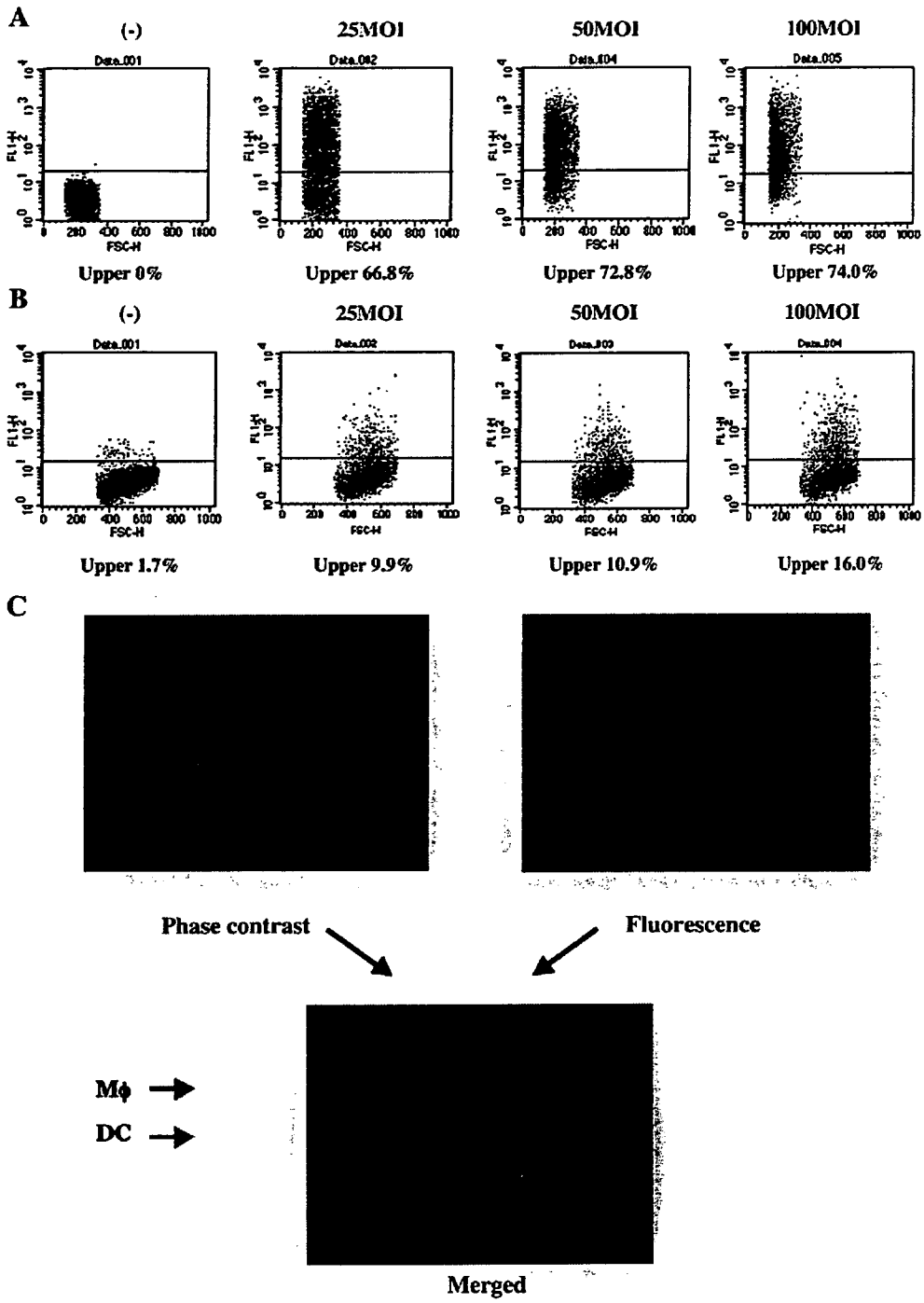

Fig. 3. Flowcytometric analysis of PEM and DC treated with EGFP-adenoviral vectors. (A) PEM and (B) DC-enriched cell population was subjected to EGFP transduction for five days by adenoviral vector (Adv/EGFP) with MOI titers of 25 to 100. (C) It displays cytospin picture taken from DC-enriched cell population treated by Adv/EGFP with 100 MOI.

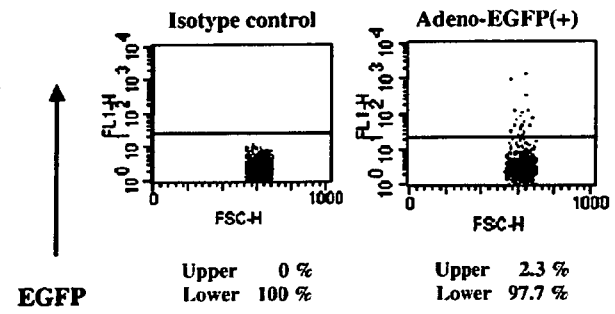

Fig. 4. Flowcytometric analysis of CD161a+ DC treated with EGFP-adenoviral vectors. CD161a+ DC were prepared from a long-term culture of rat BMC driven by Flt3/Flk2 ligand and IL-6 and separated positively by an AutoMACS system. CD161a+ DC were prepared on day 21 and treated with 100 MOI for five days.

CD161a (NKR-P1A, Natural Killer Receptor-Protein 1A gene product), a known marker of rat natural killer cells, along with other representative co-accessory molecules such as CD80 and CD86.

Unlike CD161a+ DC driven by Flt3/Flk2 ligand, CD3−CD4+ peritoneal exudate cells (that have been depleted of CD3 positive cells and then positively selected by CD4) belong to a subset of macrophages (PEM) [30] with a high level of CD4 marker along with CD11b/c and relatively weak expression of class II molecules.

4.1. Rat cardiac transplantation

We will address the functional modification of EGFP-expressing APC based on the EGFP-transduction systems. Thus EGFP-transgenic cardiac isografts as a tumor model, the fate of cardiac grafting between EGFP-transgenic and non-transgenic littermates was examined.

As shown in Table 1, EGFP-expressing cardiac isografts were accepted by non-transgenic littermates whereas skin isografts were not (data not shown).

Priming effects on cardiac isografts by EGFP-transduced APC were further examined employing lentivirally EGFP-transduced DC (lenti-DC, Group 2a) and PEM (lenti-PEM, Group 2b).

Under the optimized transductive conditions described below both lentiviral EGFP-transduced DC (lenti-DC) and PEM (lenti-PEM) were found to induce EGFP-transgenic cardiac isograft rejection, although the former was significantly more effective than the latter (Fig. 2. Group 2a versus Group 2b, $p=0.029$: see summary in Table 2). Relative efficiency of lentiviral EGFP-transduction in DC (lenti-DC) and PEM (lenti-PEM) is shown in Figs. 5, 6A, 7B and 8, respectively.

Thus lentivirally EGFP-transduced DC (lenti-DC) were able to cause non-transgenic littermates to reject EGFP-transgenic isografts (MST: 13 days). Likewise, lentivirally EGFP-transduced PEM (lenti-PEM) did the same for EGFP-transgenic isografts (MST: 23 days in Tables 1 and 2).

However, unlike PEM (adeno-PEM) with high transduction efficiency by EGFP-adenoviral vector systems (Group 3c, MST: 12 days, and also see Fig. 3A), neither adenoviral: adeno-mDC (Group 3b, Fig. 4) nor lentiviral: lenti-mDC (Group 3a, Fig. 7A) vector system was able to transduce EGFP directly into purified DC. Thus CD161a+ DC treated by lentiviral-(lenti-mDC) or adenoviral (adeno-mDC) EGFP vectors failed to sensitize the non-transgenic littermates against transgenic EGFP-cardiac isografts (Tables 1 and 2). When the fully mature DC with CD161a marker were employed for EGFP-transduction, biologically significant transduction in mature DC appeared to be not observed.

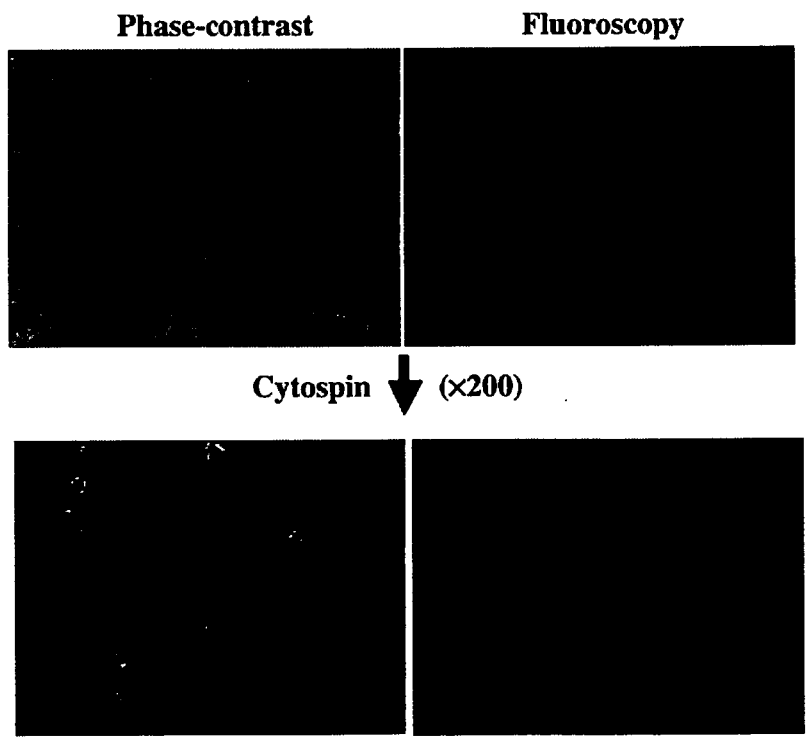

Fig. 5. Photograph of DC during culture and its cytospin feature. EGFP-lentiviral vector systems were applied to a long-term culture of rat bone marrow cells (BMC) to generate DC by cytokine combinations of Flt3/Flk2 ligand and IL-6. Photograph was taken from the culture flask of phase-contrast microscopy and fluoroscopy (upper × 100). Cytospin photograph of phase-contrast microscopy and fluoroscopy (lower × 200). Bold red arrows show a typical veiled form of DC.

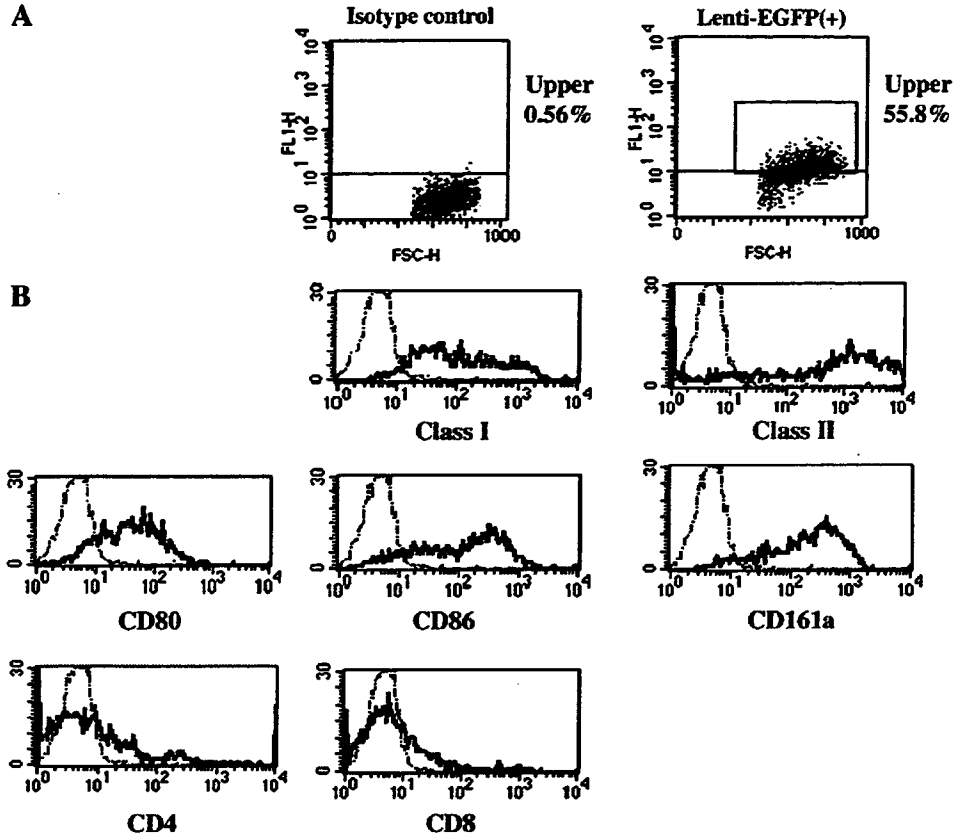

Fig. 6. Phenotypical analysis of lentivirally EGFP-transduced DC. Lenti-EGFP of two MOI were mixed with rat BMC during three weeks' culture (on day 7 and on day 14 as described in Materials and methods). EGFP transduced DC on day 21 were analyzed by flow cytometry. Flow cytometry of EGFP expressing rat DC was demonstrated against different cell surface markers including class I, class II, CD80, CD86, CD161a, CD4 and CD8a.

In contrast to studies reported by others [17,18], it appears that there has been no direct evidence to support the view that fully mature DC are able to transduce exogenous gene. We will examine and present experiment conditions employed in current study regarding how gene modification occurred in developing DC progenitors by viral vectors inasmuch as gene modification of mature DC did not occur commonly.

4.2. Gene transduction into DC and PEM target cells using the EGFP reporter gene with two viral vector systems

Gene transduction efficiency was examined for two viral vector systems based on our previous reports [20].

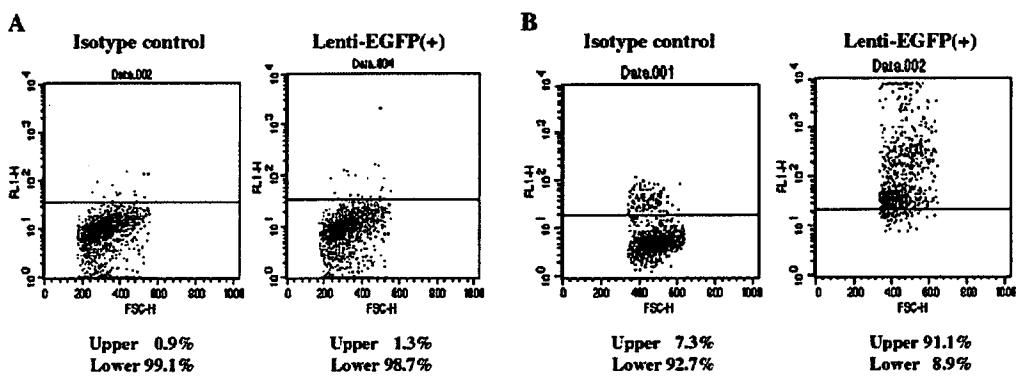

Fig. 7. Flowcytometric analysis of lentiviral EGFP gene transduction to rat mature DC and developing DC. (A) Purified mature DC were treated with 5 MOI of lentiviral vectors. Purified mature DC indicate CD161a (NKR-P1A)-positive DC separated by an AutoMACS system. (B) Developing DC progenitors treated with EGFP-lentiviral vector. DC were generated from a long-term culture of rat BMC driven by Flt3/Flk2 ligand, IL-6 and EGFP-lentiviral vectors. Lenti-EGFP of two MOI was added at week-interval (on day 7 and day 14). Flowcytometry was analyzed on day 21. Transduction efficiency (84%, treated with total ten MOI) was better than in Fig. 6A (55%, treated with total four MOI) because of the higher total MOI. However, cell viability was worse than in Fig. 6A because of its cytotoxicity (data not shown).

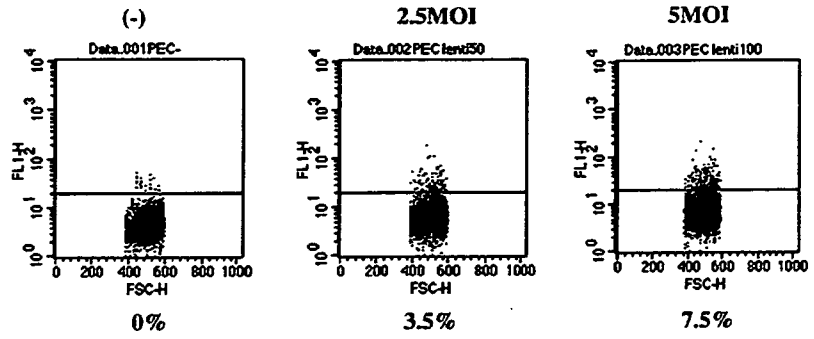

Fig. 8. Flowcytometry of rat PEM treated with EGFP-lentiviral vector. PEM were treated with EGFP-lentiviral vector systems (2.5 to 5 MOI for two weeks' treatment), and flowcytometric assay was performed. It displays forward scatter (cell size) versus fluorescence intensity (FL1).

4.3. Adenovirus-based EGFP vector

DC-generating culture systems on day 21 and peritoneal exudate cells (PEC) containing CD4+ macrophages were incubated with the vector encoding EGFP (Adeno-EGFP) at multiplicities of infection (MOI) values from 25 to 100 for five days. Fluorescence intensity versus cell size (forward scatter) is shown (Fig. 3A and B). The gene transduction rate on day 2 increased proportionally to the adenoviral MOI value. With an MOI value of 100 on day 5, expression of DC culture was 16% (Fig. 3B), whereas that of PEM was determined to be 74% by FACS analysis (Fig. 3A). Cytospin analysis of DC treated by adenoviral EGFP vector (Adv/EGFP) revealed that EGFP positive cells did not belong bona fide DC (Fig. 3C). Based on the cytological analysis, these cells were not employed for EGFP-priming experiments.

Nevertheless, the EGFP-expressing DC were found to be nearly zero when the DC were separated by CD161a surface marker (Fig. 4).

It should be noted that viral vectors are cytotoxic in general, and the adenoviral vector system appeared to be highly cytotoxic to DC at high MOIs of 100 or more. Most of the target DC died within seven to nine days following the introduction of adenoviral vector into the culture system. In contrast, the viability of the DC was still high when the adenoviral vector system was not added to the culture systems (data not shown).

4.4. HIV-1 based lentiviral vector

For the DC-generating culture described in Materials and methods, EGFP expression was observed under a phase-contrast fluorescence microscope from day 14 to day 21 with the two to five MOI treatments (Fig. 5 taken on day 21 by total ten MOI). Gene expression was apparent and stronger after day 14. Flowcytometric analysis of lentiviral EGFP treated BMC culture (Fig. 7B) also revealed that the gated EGFP positive cell populations (Fig. 6A) belonged to CD161a+ as well as class I+, class II+, CD80+, and CD86+ cells (Fig. 6B). Cytospin analysis also revealed that EGFP is indeed induced in veiled form of bona fide DC (Fig. 5).

However, the EGFP transduction was not detected by flowcytometric analysis when CD161a+ mature DC driven by Flt3/Flk2 ligand and Il-6 were employed for the EGFP-lentiviral vector systems (Fig. 7A for CD161a+ mature DC targets versus Fig. 7B for developing DC progenitors).

It appears that fully mature DC (mDC) are highly resistant or impossible to transduce by the two representative viral vectors currently available under strict experiment conditions.

When PEM that had been purified with CD3 and CD4 markers described in Materials and methods (i.e., CD3−CD4+ selection) were targeted with EGFP-lentiviral vector systems (2.5 to 5 MOI for two weeks' treatment), a low level of EGFP induction occurred, however, significant dose-dependent EGFP transduction was observed (Fig. 8).

All these data reveal that EGFP was only transduced into a subset of developing DC progenitors not into fully mature DC (mDC).

5. Discussion

Dendritic cells (DC) and a subset of macrophages that belongs to specialized antigen presenting cells (APC) play pivotal roles in initiating primary immune response [8]. Therefore, it is likely that gene-modified DC are able to affect immune response and provide a powerful tool in the study of immunotherapy of infection, cancer, and organ transplantation. As demonstrated in this study, EGFP-transduced DC as well as PEM, were able to sensitize non-transgenic littermates to transgenic EGFP that behaves as a minor histocompatibility antigen.

Regarding the functional aspects of EGFP-transduced DC and PEM when it applies to transplantation immunology in particular, both transgenic EGFP and transduced EGFP appear to behave as typical TAA or minor histocompatibility antigens. This indicates that the transgenic EGFP antigen is an important target for cell-mediated immunity and may not be a main target of humoral immunity. Our study demonstrated that both EGFP-transduced DC and PEM caused non-transgenic littermates to be primed to EGFP-transgenic cardiac isografts. The non-transgenic littermates were unable to reject the EGFP-transgenic primary cardiac isografts unless they were sensitized by EGFP-transduced APC. Thus, both developing DC progenitors and freshly isolated PEM were able to be transduced with the EGFP and enable non-transgenic littermates to reject EGFP-transgenic cardiac isografts. However, this priming effect was not observed when the fully mature DC (mDC) were employed for the target cells of the viral gene transduction.

In contrast to other studies [13,33], our results indicate that direct gene transduction and functional expression of exogenous genes into mature DC do not commonly occur. In this study, we confirmed and extended our previous finding that when a subset of highly purified mature DC (CD161a+ DC), was employed, neither adenoviral nor lentiviral vector systems for transduction methods applied here were able to transduce and express the reporter gene EGFP in DC [20]. In contrast, when either developing DC progenitor cells or PEM were used

as the target cells with the viral vectors, they could successfully transduce the EGFP gene into *bona fide mature DC* as well as PEM. However, a comparison between the lentiviral and adenoviral vector systems indicates that the lentiviral vector system is more suitable for transduction into developing DC due to the low cytotoxicity (data not shown).

Although the lentiviral vector is useful for the transduction of exogenous genes in terminally differentiated non-dividing cells, such as neuronal [26], hepatic and muscular cells [34], this is not the case with *fully mature rat DC* (*mDC*). Even with the lentiviral vector, successful gene transduction only occurred in dividing *DC progenitor cells*. Thus gene transduction of terminally differentiated cells occurs less commonly in non-dividing and end-stage mature DC. The results obtained in this study agree with the findings of other studies demonstrating that the lentiviral gene-transfer methods for hematopoietic stem cells are among the most efficient methods currently available [35].

In this study, we addressed a simple issue: whether and to what extent two viral vector systems are able to affect the transduction of genes into a subset of purified DC. Based on our previous studies, gene transduction into DC should be clarified and should be divided into at least two stages. One stage is gene transduction for developing DC progenitor cells (dividing cells) during the culture with cytokines. The other stage is for terminally differentiated mature DC (non-dividing cells). For terminally differentiated DC, the adenoviral vector is expected to transduce genes into non-dividing DC. However, gene expression was not verified phenotypically or functionally in mature DC under carefully conditioned systems. To accomplish a high level of gene transfer into mouse DC using adenoviral vectors, it has been claimed that high titers of MOI had to be maintained within a range of 50 to 1000. In our study, successful gene transduction into bona fide DC did not occur although adenoviral vector was able to transduce the EGFP gene into a DC-containing cell population. This was further demonstrated by re-analyzing the purified CD161a (+) DC. This observation strongly suggests that, although adenoviral vectors can be used to facilitate transduction in DC progenitor cells and/or DC like macrophages, they fail to transduce genes into CD161a (+) DC (i.e. fully *mature bona fide DC:mDC*). The reason for this is currently unknown. Furthermore, it has been shown that adenoviral vector requires virus specific receptor called CAR (coxsackie adenoviral receptor) for a virus attachment to the target cells [36]. Inasmuch as the expression of CAR are not ubiquitous among the target cells, CAR negative target cells such as DC and lymphocytes may not be able to transduce the genes. In this regard a new type of adenoviral vector bearing RGD (arginine-glycine-aspartic acid) motif that binds alpha v beta3 integrin ($\alpha V\beta 3$:CD51, CD61) and mediates virus internalization, has been developed [37]. Since this family of integrins is more widely distributed to the target cell surface including DC cell lines from both human and mouse, it was shown that the fiber modified adenoviral vectors were more efficient for the gene transduction into those cell lines than that of original vector [38,39]. However, our preliminary study demonstrated that this is not the case. In contrast to these studies a significant gene transduction did not occur in the *bona fide* DC as described in this study even with a new type of fiber modified adenoviral vector encoding EGFP (Adv-F/RGD-EGFP). The reason for this discrepancy is currently unknown. However, it is tempting to suggest that it could be due to the unique function of DC as a specialized APC. Inasmuch as DC are specialized cells responsible as primary defense called innate immunity. DC might be equipped with special molecular machinery including an array of toll-like receptors that does not allow viral replication [40]. Furthermore, the high level of Interferon expression in DC might also interfere with the function of viral vector [41–44].

Onco-retroviral vector systems are the most popular vector systems currently used in gene therapy studies. However, onco-retroviral vector systems and plasmid vector systems in general are only able to transduce genes into dividing cells [9–12]. Therefore, the lentiviral vector system used in this study was developed as an improved substitute for retroviral vector systems capable of transducing genes into non-dividing cells. This new, third-generation lentiviral vector is far safer than the earlier versions. This study demonstrates that this lentiviral vector is used to successfully transduce EGFP genes into a population of developing DC progenitors. Nevertheless, when *bona fide* DC selected by CD161a surface marker were used, the vector could not facilitate the transduction of genes into the target DC.

Although the precise definition of DC subsets such as plasmacytoid DC and myeloid DC, in particular phenotypic or functional maturity of CD161a+ DC must await further analysis, our study represents the first report to provide evidence that EGFP is transduced in *bona fide* DC not in a subset of macrophages. Most, if not all, gene-transfer studies dealing with DC appear to employ heterogeneous cell populations, usually DC-like macrophages. As demonstrated in this study, vector systems with EGFP reporters were unable to transduce sufficient genes into CD161a+ DC directly. Further studies of the viral transduction mechanism and analysis of DC function might ultimately lead to the development of improved methods useful for several clinical applications.

In conclusion, the lentiviral vector system was the most effective method for gene transduction in developing DC progenitors. The efficient transduction of the EGFP gene was verified by the ability of the EGFP-transduced DC to cause non-transgenic littermates to reject EGFP-transgenic cardiac isografts. Phenotypic and functional EGFP gene expression was likewise observed in a unique subset of macrophages in PEC by both lenti- and adenoviral vector systems.

Acknowledgements

We are grateful to Amgen Inc. for supplying rat c-kit ligand and to Kirin Brewer Company Ltd. for generous gifts of human recombinant IL-6. We also thank: Drs. Hideo Yagita, Masayuki Miyasaka for providing the useful monoclonal antibodies.

References

[1] Chalfie M, Tu Y, Euskirchen G, Ward WW, Prasher DC. Green fluorescent protein as a marker for gene expression. Science 1994;263 (5148):802–5.

[2] Townsend AR, Rothbard J, Gotch FM, Bahadur G, Wraith D, McMichael AJ. The epitopes of influenza nucleoprotein recognized by cytotoxic T lymphocytes can be defined with short synthetic peptides. Cell 1986;44(6):959–68.
[3] Moore MW, Carbone FR, Bevan MJ. Introduction of soluble protein into the class I pathway of antigen processing and presentation. Cell 1988;54(6):777–85.
[4] Wallny HJ, Rammensee HG. Identification of classical minor histocompatibility antigen as cell-derived peptide. Nature 1990;343(6255):275–8.
[5] Scott DM, Ehrmann IE, Ellis PS, Bishop CE, Agulnik AI, Simpson E, et al. Identification of a mouse male-specific transplantation antigen, H–Y. Nature 1995;376(6542):695–8.
[6] Simpson E, Matsunaga T, Brenan M, Brunner C, Benjamin D, Hetherington C, et al. H–Y antigen as a model for tumor antigens: the role of H-2-associative antigens in controlling anti-H–Y immune responses. Transplant Proc 1980;12(1):103–6.
[7] Simpson E, Roopenian D, Goulmy E. Much ado about minor histocompatibility antigens. Immunol Today 1998;19(3):108–12.
[8] Nussenzweig MC, Steinman RM. Contribution of dendritic cells to stimulation of the murine syngeneic mixed leukocyte reaction. J Exp Med 1980;151(5):1196–212.
[9] Storek J, Kiem HP. Transgene expression by a large fraction of dendritic cells following autologous transplantation of retrovirally transduced CD34 cells. Stem Cells Dev 2006;15(5):619–21.
[10] Cui Y, Kelleher E, Straley E, Fuchs E, Gorski K, Levitsky H, et al. Immunotherapy of established tumors using bone marrow transplantation with antigen gene-modified hematopoietic stem cells. Nat Med 2003;9(7):952–8.
[11] Temme A, Morgenroth A, Schmitz M, Weigle B, Rohayem J, Lindemann D, et al. Efficient transduction and long-term retroviral expression of the melanoma-associated tumor antigen tyrosinase in CD34(+) cord blood-derived dendritic cells. Gene Ther 2002;9(22):1551–60.
[12] Reeves ME, Royal RE, Lam JS, Rosenberg SA, Hwu P. Retroviral transduction of human dendritic cells with a tumor-associated antigen gene. Cancer Res 1996;56(24):5672–7.
[13] Lu L, Gambotto A, Lee WC, Qian S, Bonham CA, Robbins PD, et al. Adenoviral delivery of CTLA4Ig into myeloid dendritic cells promotes their in vitro tolerogenicity and survival in allogeneic recipients. Gene Ther 1999;6(4):554–63.
[14] Nishimura N, Nishioka Y, Shinohara T, Ogawa H, Yamamoto S, Tani K, et al. Novel centrifugal method for simple and highly efficient adenovirus-mediated green fluorescence protein gene transduction into human monocyte-derived dendritic cells. J Immunol Methods 2001;253(1–2):113–24.
[15] Takayama T, Nishioka Y, Lu L, Lotze MT, Tahara H, Thomson AW. Retroviral delivery of viral interleukin-10 into myeloid dendritic cells markedly inhibits their allostimulatory activity and promotes the induction of T-cell hyporesponsiveness. Transplantation 1998;66(12):1567–74.
[16] Kaneda Y. Development of a novel fusogenic viral liposome system (HVJ-liposomes) and its applications to the treatment of acquired diseases. Mol Membr Biol 1999;16(1):119–22.
[17] Kaneda Y, Nakajima T, Nishikawa T, Yamamoto S, Ikegami H, Suzuki N, et al. Hemagglutinating virus of Japan (HVJ) envelope vector as a versatile gene delivery system. Mol Ther 2002;6(2):219–26.
[18] Van Tendeloo VF, Snoeck HW, Lardon F, Vanham GL, Nijs G, Lenjou M, et al. Nonviral transfection of distinct types of human dendritic cells: high-efficiency gene transfer by electroporation into hematopoietic progenitor—but not monocyte-derived dendritic cells. Gene Ther 1998;5(5):700–7.
[19] Lenz P, Bacot SM, Frazier-Jessen MR, Feldman GM. Nucleoporation of dendritic cells: efficient gene transfer by electroporation into human monocyte-derived dendritic cells. FEBS Lett 2003;538(1–3):149–54.
[20] Satoh E, Hara Y, Fuji N, Li XK, Teramoto K, Arii S, et al. Comparison of the vector systems for gene transduction into rat dendritic cells and peritoneal exudate cells. Transplant Proc 2005;37(4):1953–6.
[21] Matsue H, Matsue K, Walters M, Okumura K, Yagita H, Takashima A. Induction of antigen-specific immunosuppression by CD95L cDNA-transfected 'killer' dendritic cells. Nat Med 1999;5(8):930–7.
[22] Dietz AB, Vuk-Pavlovic S. High efficiency adenovirus-mediated gene transfer to human dendritic cells. Blood 1998;91(2):392–8.
[23] Boonstra A, Asselin-Paturel C, Gilliet M, Crain C, Trinchieri G, Liu YJ, et al. Flexibility of mouse classical and plasmacytoid-derived dendritic cells in directing T helper type 1 and 2 cell development: dependency on antigen dose and differential toll-like receptor ligation. J Exp Med 2003;197(1):101–9.
[24] Hua Y, Miyagi T, Saito H, Gold DP, Li XK, Fujino M, et al. Cytokine requirement for the development of rat dendritic cells by in vitro culturing of bone marrow cells. Transplant Proc 2000;32(7):2078–9.
[25] Yan H, Miyagi T, Satoh E, Sugiura W, Yamamoto N, Kimura H. Phenotype and function of GM-CSF independent dendritic cells generated by long-term propagation of rat bone marrow cells. Cell Immunol 2004;229(2):117–29.
[26] Naldini L, Blomer U, Gage FH, Trono D, Verma IM. Efficient transfer, integration, and sustained long-term expression of the transgene in adult rat brains injected with a lentiviral vector. Proc Natl Acad Sci U S A 1996;93(21):11382–8.
[27] Miyoshi H, Blomer U, Takahashi M, Gage FH, Verma IM. Development of a self-inactivating lentivirus vector. J Virol 1998;72(10):8150–7.
[28] Hasuwa H, Kaseda K, Einarsdottir T, Okabe M. Small interfering RNA and gene silencing in transgenic mice and rats. FEBS Lett 2002;532(1–2):227–30.
[29] Ono K, Lindsey ES. Improved technique of heart transplantation in rats. J Thorac Cardiovasc Surg 1969;57(2):225–9.
[30] Jefferies WA, Green JR, Williams AF. Authentic T helper CD4 (W3/25) antigen on rat peritoneal macrophages. J Exp Med 1985;162(1):117–27.
[31] Miyake S, Makimura M, Kanegae Y, Harada S, Sato Y, Takamori K, et al. Efficient generation of recombinant adenoviruses using adenovirus DNA-terminal protein complex and a cosmid bearing the full-length virus genome. Proc Natl Acad Sci U S A 1996;93(3):1320–4.
[32] Sprent J, Schaefer M. Antigen-presenting cells for Lyt-2+ cells. II. Primary mixed-lymphocyte reactions stimulated by Ia+ dendritic cells and Ia- peritoneal exudate cells. Int Immunol 1989;1(5):517–25.
[33] Nishioka Y, Hirao M, Robbins PD, Lotze MT, Tahara H. Induction of systemic and therapeutic antitumor immunity using intratumoral injection of dendritic cells genetically modified to express interleukin 12. Cancer Res 1999;59(16):4035–41.
[34] Kafri T, Blomer U, Peterson DA, Gage FH, Verma IM. Sustained expression of genes delivered directly into liver and muscle by lentiviral vectors. Nat Genet 1997;17(3):314–7.
[35] Miyoshi H. Gene delivery to hematopoietic stem cells using lentiviral vectors. Methods Mol Biol 2004;246:429–38.
[36] Bergelson JM, Cunningham JA, Droguett G, Kurt-Jones EA, Krithivas A, Hong JS, et al. Isolation of a common receptor for Coxsackie B viruses and adenoviruses 2 and 5. Science 1997;275(5304):1320–3.
[37] Mizuguchi H, Koizumi N, Hosono T, Utoguchi N, Watanabe Y, Kay MA, et al. A simplified system for constructing recombinant adenoviral vectors containing heterologous peptides in the HI loop of their fiber knob. Gene Ther 2001;8(9):730–5.
[38] Okada N, Tsukada Y, Nakagawa S, Mizuguchi H, Mori K, Saito T, et al. Efficient gene delivery into dendritic cells by fiber-mutant adenovirus vectors. Biochem Biophys Res Commun 2001;282(1):173–9.
[39] Okada N, Masunaga Y, Okada Y, Iiyama S, Mori N, Tsuda T, et al. Gene transduction efficiency and maturation status in mouse bone marrow-derived dendritic cells infected with conventional or RGD fiber-mutant adenovirus vectors. Cancer Gene Ther 2003;10(5):421–31.
[40] Kaisho T, Akira S. Dendritic-cell function in Toll-like receptor- and MyD88-knockout mice. Trends Immunol 2001;22(2):78–83.
[41] Vremec D, O'Keeffe M, Hochrein H, Fuchsberger M, Caminschi I, Lahoud M, et al. Production of interferons by dendritic cells, plasmacytoid cells, natural killer cells, and interferon-producing killer dendritic cells. Blood 2007;109(3):1165–73.
[42] Hochrein H, Shortman K, Vremec D, Scott B, Hertzog P, O'Keeffe M. Differential production of IL-12, IFN-alpha, and IFN-gamma by mouse dendritic cell subsets. J Immunol 2001;166(9):5448–55.
[43] Mohty M, Vialle-Castellano A, Nunes JA, Isnardon D, Olive D, Gaugler B. IFN-alpha skews monocyte differentiation into Toll-like receptor 7-expressing dendritic cells with potent functional activities. J Immunol 2003;171(7):3385–93.
[44] Mailliard RB, Wankowicz-Kalinska A, Cai Q, Wesa A, Hilkens CM, Kapsenberg ML, et al. alpha-type-1 polarized dendritic cells: a novel immunization tool with optimized CTL-inducing activity. Cancer Res 2004;64(17):5934–7.

7096–7108 Nucleic Acids Research, 2007, Vol. 35, No. 21
doi:10.1093/nar/gkm750

Published online 16 October 2007

Deaminase-independent inhibition of HIV-1 reverse transcription by APOBEC3G

Yasumasa Iwatani[1,2], Denise S.B. Chan[3], F. Wang[4], Kristen Stewart Maynard[5], Wataru Sugiura[2], Angela M. Gronenborn[3], Ioulia Rouzina[6], Mark C. Williams[4], Karin Musier-Forsyth[5,7] and Judith G. Levin[1,*]

[1]Laboratory of Molecular Genetics, National Institute of Child Health and Human Development, National Institutes of Health, Bethesda, MD 20892, USA, [2]AIDS Research Center, National Institute of Infectious Diseases, Tokyo 208-0013, Japan, [3]Department of Structural Biology, University of Pittsburgh Medical School, Pittsburgh, PA 15260, [4]Department of Physics, Northeastern University, Boston, MA 02115, [5]Department of Chemistry, [6]Department of Biochemistry, Molecular Biology, and Biophysics, University of Minnesota, Minneapolis, MN 55455 and [7]Department of Chemistry and Department of Biochemistry, Ohio State University, Columbus, OH 43210, USA

Received August 7, 2007; Revised and Accepted September 10, 2007

ABSTRACT

APOBEC3G (A3G), a host protein that inhibits HIV-1 reverse transcription and replication in the absence of Vif, displays cytidine deaminase and single-stranded (ss) nucleic acid binding activities. HIV-1 nucleocapsid protein (NC) also binds nucleic acids and has a unique property, nucleic acid chaperone activity, which is crucial for efficient reverse transcription. Here we report the interplay between A3G, NC and reverse transcriptase (RT) and the effect of highly purified A3G on individual reactions that occur during reverse transcription. We find that A3G did not affect the kinetics of NC-mediated annealing reactions, nor did it inhibit RNase H cleavage. In sharp contrast, A3G significantly inhibited *all* RT-catalyzed DNA elongation reactions with or without NC. In the case of (−) strong-stop DNA synthesis, the inhibition was independent of A3G's catalytic activity. Fluorescence anisotropy and single molecule DNA stretching analyses indicated that NC has a higher nucleic acid binding affinity than A3G, but more importantly, displays faster association/disassociation kinetics. RT binds to ssDNA with a much lower affinity than either NC or A3G. These data support a novel mechanism for deaminase-independent inhibition of reverse transcription that is determined by critical differences in the nucleic acid binding properties of A3G, NC and RT.

INTRODUCTION

Human APOBEC3G (A3G) is a host cytidine deaminase, which was first identified by Sheehy *et al.* (1) as the cellular factor that blocks HIV-1 replication in the absence of the viral Vif protein. Cellular expression of A3G results in its incorporation into *vif*-deficient HIV-1 particles, whereas its presence in WT virions is dramatically reduced by Vif-induced degradation via the ubiquitination-proteosome pathway (2).

Initial studies suggested that the deamination activity of A3G contributes to its antiviral activity and is associated with G to A hypermutation (3–6). However, more recent results indicate that a deaminase-independent mechanism might also be involved in A3G's antiviral activity: (i) Deamination activity is not absolutely correlated with antiviral activity against HIV-1 (7–15); (ii) Several reports (though not all) indicate that hepatitis B virus may be inhibited by A3G without significant detection of G to A hypermutation (16–18) and (iii) Other APOBEC proteins block replication of mouse mammary tumor virus (19) and several retrotransposons (14,20–24) in the absence of editing activity.

Prior to the discovery of A3G, it was already known that Δ*vif* viruses produced in 'nonpermissive' cells (PBMCs or certain T-cell lines, e.g. H9) were 100- to

*To whom correspondence should be addressed. Tel: +1 301 496 1970; Fax: +1 301 496 0243; Email: levinju@mail.nih.gov

© 2007 The Author(s)
This is an Open Access article distributed under the terms of the Creative Commons Attribution Non-Commercial License (http://creativecommons.org/licenses/by-nc/2.0/uk/) which permits unrestricted non-commercial use, distribution, and reproduction in any medium, provided the original work is properly cited.

1000-fold less infectious than WT (25–27) and were deficient in their ability to complete reverse transcription (28–31). Moreover, similar results were obtained in endogenous reverse transcription assays (30,32,33). More recent analysis of HIV-1-infected cells expressing A3G or A3F has confirmed the initial observations (5,10,13,15,34–38).

Efficient and specific reverse transcription depends on the viral nucleocapsid protein (NC), which functions as a nucleic acid chaperone (39–43). This means that NC can catalyze nucleic acid conformational rearrangements that lead to the most thermodynamically stable structures (44). Like NC, A3G has two zinc finger domains and binds nucleic acids (45). However, whereas A3G has a strong preference for binding single-stranded (ss) nucleic acids (6,12), NC binds ss or double-stranded (ds) RNA and DNA (46) [for further information on NC's nucleic acid binding properties, see Ref. (47)]. The two proteins also differ in their effects on virus replication: NC acts as a positive factor, whereas A3G is an inhibitor in the absence of Vif.

We previously reported the successful preparation of highly purified, catalytically active A3G expressed in a baculovirus system and demonstrated that the availability of a pure protein (without contamination by other proteins, either host or viral) was invaluable for rigorous analysis of the biochemical properties of A3G (12). In the course of this study, we unexpectedly found that A3G does not interfere with NC binding to ssRNA (and vice versa) (12). This suggested that inhibition of reverse transcription by A3G is likely to be unrelated to an effect on NC chaperone function.

To test this hypothesis and to probe the mechanism that might be involved, we took advantage of defined biochemical assay systems that we have developed over the years for studies on viral DNA synthesis (48–51). Thus, using our highly purified A3G as well as purified NC and RT, we investigated the effect of A3G on a series of reconstituted reactions that occur during reverse transcription. This allowed us to perform an independent analysis of individual steps in the pathway, which is not possible in cell-based systems. We found that A3G inhibited all reverse transcriptase (RT)-catalyzed DNA elongation reactions, but not RNase H activity or NC's ability to promote annealing. These observations could be explained by critical differences in the binding properties of NC, A3G and RT, as measured by single-molecule DNA stretching and fluorescence anisotropy (FA). Our findings are unique and provide strong support for a novel mechanism that could account for the observed deaminase-independent A3G-mediated antiviral activity.

MATERIALS AND METHODS

Materials

Purified $tRNA_3^{Lys}$ from human placenta was obtained from Bio S&T (Lachine, Quebec, Canada). DNA and RNA oligonucleotides were purchased from Lofstrand (Gaithersburg, MD), Integrated DNA Technologies (Coralville, IA), Oligos Etc., Inc. (Wilsonville, OR). [γ-^{32}P]ATP (3000 Ci/mmol) and [α-^{32}P]dCTP (6000 Ci/mmol) were purchased from GE Healthcare (Piscataway, NJ). HIV-1 RT was obtained from Worthington Biochemical Corp. (Lakewood, NJ). Calf intestinal phosphatase, T4 polynucleotide kinase, and Vent DNA polymerase were obtained from New England Biolabs (Beverly, MA). SUPERaseIn, an RNase inhibitor, was purchased from Ambion, Inc. (Austin, TX). Recombinant wild-type HIV-1 NC (55-amino-acid form) was a generous gift from Dr Robert Gorelick and was prepared as described previously (52,53). Recombinant enzymatically active A3G and the deaminase-deficient A3G mutant (C291S) were expressed in a baculovirus expression system and purified as previously described (12). A3G preparations were confirmed to be free from contamination with RNases (data not shown) and no RNA degradation was apparent in any of the experiments (e.g. see Figure 2A).

Methods

Plasmid construction. All plasmid sequences were derived from the HIV-1 pNL4-3 clone (54). Plasmid pUL (viral insert from nt 566 to 1419) was constructed from the previously described pRUG plasmid (51).

Preparation of RNA. The DNA templates for *in vitro* RNA transcription were derived from plasmid pRUG [for transactivation response element (TAR) RNA, nucleotide(s) (nt) 1–59] or pUL (for RNA UL244, nt 113–244). DNA fragments containing both the T7 promoter and the DNA sequence equivalent to the desired vRNA were amplified by PCR using Vent DNA polymerase and the following primers: forward primer (5′-ccaatgcttaatcagtgaggc), located at the start of the *amp* gene in pUL; reverse primers, 5′-gtcctgcgtcgagagatc (RNA UL244) and 5′-gggttccctagttagccaga (TAR RNA). The DNA fragments were gel-purified and transcribed using an Ambion MEGAscript kit (Ambion Inc., Austin, TX). Gel-purified RNAs were dephosphorylated by calf intestinal phosphatase and were then labeled at their 5′ ends with [γ-^{32}P]ATP, using T4 polynucleotide kinase (55). Unincorporated nucleotides were removed by passing the reaction mixture through NucAway Spin Columns (Ambion). RNA 244 (51) and acceptor RNA 148 (49) were prepared as described.

Reverse transcription assays. Reaction components are given for 20 µl unit reactions, which were scaled up as needed. SUPERaseIn at a final concentration of 0.5 U/µl was added to all RNA-containing reaction mixtures. Incubation/preincubation was always at 37°C. Six percent native or denaturing polyacrylamide gels were used for annealing or extension assays, respectively, except as noted. Radioactivity was quantified by using a Typhoon PhosphorImager and ImageQuant software.

$tRNA_3^{Lys}$ annealing to viral RNA (vRNA). Reaction mixtures contained buffer (50 mM Tris–HCl (pH 8.0), 75 mM KCl, 0.1 mM $MgCl_2$, 1 mM DTT), 0.2 pmol of purified human placental $tRNA_3^{Lys}$ and 0.1 pmol of 5′ ^{32}P-labeled RNA UL244 and were incubated in the

absence or presence of A3G (80 nM) with or without HIV-1 NC (7 nt/NC, 0.2 μM). Prior to loading on the gel, the samples were treated with Proteinase K (0.5 mg/ml).

(−)Strong-Stop DNA [(−) SSDNA] synthesis. Template RNA 244 (0.1 pmol) and 0.1 pmol each of human $tRNA_3^{Lys}$ or ^{32}P-labeled D18 primer, [complementary to the 18-nt primer-binding site (PBS)] were heat-annealed as described (51). A3G or heat-denatured (hd)A3G was then added to buffer designated as 'reaction buffer' (50 mM Tris–HCl (pH 8.0), 75 mM KCl, 7 mM $MgCl_2$, 1 mM DTT) and the mixture was preincubated for 5 min. Primer extension was initiated by adding HIV-1 RT (0.1 pmol) and 50 μM each of dATP, dTTP and dGTP plus 10 μCi of [α-^{32}P]dCTP ($tRNA_3^{Lys}$) or 50 μM each of all four dNTPs (D18).

Annealing and minus-strand transfer. Minus-strand annealing was performed as described previously (56) in the presence or absence of A3G (80 nM) with or without HIV-1 NC (3.5 nt/NC, 0.4 μM). For minus-strand transfer assays, reaction mixtures contained the components present in annealing reactions as well as HIV-1 RT (0.4 pmol), all four dNTPs (each at 50 μM), and 1 mM $MgCl_2$.

Initiation of plus-strand DNA synthesis. The assay was performed using a modified version of a previous protocol (57). Briefly, the 15-nt polypurine tract (PPT) primer (0.2 pmol) was heat-annealed to a 35-nt minus-strand DNA template (0.1 pmol) and the hybrid was preincubated with or without A3G (80 nM) for 5 min in reaction buffer (see above). DNA synthesis was initiated by adding HIV-1 RT (0.4 pmol), all four dNTPs (each at 0.5 μM), and [α-^{32}P]dCTP (20 μCi), which results in an internally labeled DNA product. Samples were loaded on a 15% denaturing gel. Since RNase H cleavage removes the annealed 15-nt PPT RNA, the DNA product is 20 nt.

Plus-strand transfer. The assay was performed as described previously (50) except that the final concentrations of 5′ ^{32}P-labeled (+) SSDNA donor (50 nt) and minus-strand DNA acceptor (48 nt) were 5 nM, all four dNTPs were at 50 μM each, and HIV-1 RT was 20 nM. Reactions were incubated in the presence or absence of NC (3.5 nt/NC, 0.14 μM), with or without A3G (80 nM).

Single molecule DNA stretching. Purified bacteriophage lambda DNA (48 500 bp) was labeled on its 3′ ends with biotin and single DNA molecules were captured between two streptavidin-coated, 5 μm diameter polystyrene beads using a dual beam optical tweezers instrument (58,59). The 16.5 μm contour length DNA molecule was stretched in 100 nm steps using a piezoelectric flexure translation stage (Melles Griot, Carlsbad, CA) to reveal the DNA force-extension curve, as described previously (58). After stretching a single DNA molecule in DNA stretching buffer (10 mM HEPES, pH 7.5, 50 mM Na^+, at 20°C), and verifying that a single molecule was present, the buffer solution was exchanged for a solution containing the same buffer with a fixed protein concentration. The protein exchange procedure was then repeated for different protein concentrations in order to determine the effect of protein on DNA stretching behavior. The transition width and hysteresis were analyzed as described previously (60) for 3 or more DNA molecules.

FA experiments. Equilibrium binding of HIV-1 NC, HIV-1 RT and human A3G to a 6-carboxyfluorescein (FAM)-labeled 20-nt ssDNA oligonucleotide (5′-FAM-JL587D, 5′FAM-CTTCTTTGGGAGTGAAT TAG-3′) was examined using FA. The HPLC-purified oligonucleotide 5′-FAM-JL587D was purchased from TriLink Biotechnologies (San Diego, CA). FA measurements were performed on an Analyst AD plate reader system (Molecular Devices, Sunnyvale, CA) using Corning 3676 low-volume 384-well black non-binding surface polystyrene plates. Reaction mixtures contained 20 nM 5′-FAM-JL587D, varying concentrations of NC, RT or A3G, and buffer consisting of 50 mM Tris–HCl (pH 8.0), 75 mM KCl, 7 mM $MgCl_2$ and 1 mM DTT. Samples were excited at 485 nm and the emission intensities at 530 nm from the parallel and perpendicular planes were measured. Apparent equilibrium dissociation constants (K_d) were determined by plotting the FA signal, A, as a function of protein concentration, C. The data were fit assuming 1:1 oligomer:protein binding using the expression (61,62):

$$A(C) = \frac{A_F + \Theta \cdot (A_B R - A_F)}{\Theta \cdot (R-1) + 1}$$

where

$$\Theta = \frac{1}{2D} \cdot \left[D + C + K_d - \sqrt{(D + C + K_d)^2 - 4C \cdot D} \right]$$

is the fraction of oligonucleotides bound, D is the oligonucleotide strand concentration, and A_B and A_F are the anisotropy values of the fully bound and unbound oligonucleotides, respectively. R is the ratio of the fluorescence intensity of saturated bound oligonucleotide relative to free oligonucleotide, which accounts for changes in fluorescence intensity upon protein binding (46,47,61).

RESULTS

Effect of A3G on primer placement and (−) SSDNA synthesis

To determine the mechanism by which A3G inhibits HIV-1 DNA synthesis, we analyzed the effect of A3G on single steps in the reverse transcription pathway (Figure 1) (43). Annealing and DNA synthesis were assayed in a series of reconstituted model systems. Our goal was to determine whether A3G interfered with the nucleic acid chaperone activity of NC, the catalytic activity of RT, or both during these reactions. Note that in most of the assays, the concentration of A3G did not exceed 80 nM, since A3G precipitates at high concentrations (12).

To evaluate the effect of A3G on the first step in reverse transcription (primer placement), we investigated

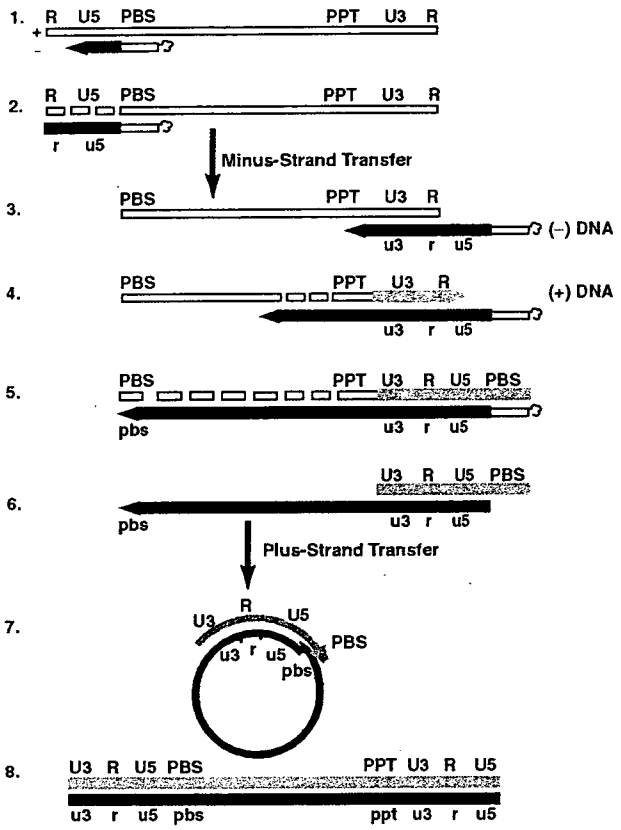

Figure 1. Schematic diagram of the events in reverse transcription. Step 1. Reverse transcription is initiated by a cellular tRNA primer ($tRNA_3^{Lys}$, in the case of HIV-1), following annealing of the 3′ 18 nt of the tRNA to the 18-nt PBS near the 5′ end of the genome. RT catalyzes synthesis of (−) SSDNA, which contains copies of the R sequence and the unique 5′ genomic sequence (U5). Step 2. As the primer is extended, the RNase H activity of RT degrades the genomic RNA sequences that have been reverse transcribed. Step 3. (−) SSDNA is transferred to the 3′ end of vRNA (minus-strand transfer). Step 4. Elongation of minus-strand DNA and RNase H degradation continue. Plus-strand synthesis is initiated by the 15-nt PPT immediately upstream of the unique 3′ genomic sequence (U3). Step 5. RT copies the u3, u5 and r regions in minus-strand DNA, as well as the 3′ 18 nt of the tRNA primer, thereby reconstituting the PBS. The product formed is termed (+) SSDNA. Step 6. RNase H removal of the tRNA and PPT primers from minus- and plus-strand DNAs, respectively. Step 7. Plus-strand transfer, facilitated by annealing of the complementary PBS sequences at the 3′ ends of (+) SSDNA and minus-strand DNA, is followed by circularization of the two DNA strands and displacement synthesis. Step 8. Minus- and plus-strand DNAs are elongated, resulting in a linear dsDNA with a long terminal repeat (LTR) at each end. vRNA is shown by an open rectangle and minus-and plus-strand DNAs are shown by black and gray rectangles, respectively. The tRNA primer is represented by a short open rectangle (3′ 18 nt of the tRNA) attached to a 'clover-leaf' (remaining tRNA bases). Minus- and plus-strand sequences are depicted in lower and upper case, respectively. The very short white rectangles represent fragments produced by RNase H cleavage of genomic RNA. Adapted from reference (43) with permission from Elsevier.

the time course of NC-dependent annealing of human $tRNA_3^{Lys}$ to the PBS in a short vRNA template (RNA UL244) (Figure 2A and B). In the absence of NC and A3G, no annealing was detected. As shown in Figure 2B, the rates of annealing in the presence of NC were similar for reactions with and without A3G and the end point values at 64 min were 70% and 66%, respectively. Addition of NC and hdA3G resulted in a slightly enhanced rate of annealing, but the end point value was very close to the values with and without native A3G. These results demonstrate that A3G did not interfere with NC-mediated formation of the vRNA–tRNA complex.

Primer placement is followed by extension of $tRNA_3^{Lys}$ and synthesis of (−) SSDNA (Figure 1, steps 1 and 2). To measure extension alone, the tRNA was first heat annealed to the vRNA 244 template (51); the (−) SSDNA product formed by addition of RT was internally labeled (Figure 2C) (51). In the absence of A3G (lane 1) or in the presence of hdA3G (lanes 2–4), equivalent amounts of the 258-nt full-length product [(−) SSDNA attached to $tRNA_3^{Lys}$] and pause products (including the initial +1, +3 and +5 DNAs) were detected. However, in the presence of increasing amounts of native A3G (20–80 nM) (lanes 5–7), the amounts of fully extended product and pause products were greatly reduced; with 80 nM A3G, only the +1 and +5 DNAs could be detected (lane 7). Furthermore, some of the pause products observed in the presence of A3G differed from those made in the absence of the inhibitor (compare lanes 2–4 with lanes 5 and 6). Taken together, these results indicate that native A3G strongly inhibited tRNA-primed (−) SSDNA synthesis.

To investigate the kinetics of (−) SSDNA synthesis in the presence of increasing amounts of A3G, we used 5′ ^{32}P-labeled D18 in place of tRNA (Figure 3A). This allowed us to obtain quantitative data, which were plotted as the percent of (−) SSDNA in total DNA products [% (−) SSDNA] versus Time (Figure 3B). In accord with the tRNA experiment Figure 2C), A3G reduced (−) SSDNA synthesis in a dose-dependent manner (Figure 3A and B). For example, at 64 min, the relative amount of (−) SSDNA synthesized in the 80 nM reaction was decreased by 24-fold compared with the minus A3G value. In addition, as also shown in Figure 2C, we observed changes in the pausing pattern in A3G-containing reactions, which were accentuated with increasing concentrations of A3G (Figure 3A). Interestingly, mapping these sites on the RNA 244 template structure (51) indicated that the pause sites occurred near or within ss regions in the template (see Figure 3C, which was derived from the gel data in Figure S1). This is consistent with A3G's well-documented, strong preference for binding to ss nucleic acids (6,12).

The data in Figures 2 and 3 demonstrate that A3G dramatically suppressed (−) SSDNA synthesis primed by either $tRNA_3^{Lys}$ or D18. The results with D18 also suggest that the reduction of tRNA-primed (−) SSDNA synthesis by A3G was not due to an altered configuration of the tRNA/vRNA initiation complex. Interestingly, when 6-fold less RNA template was used, 20 nM of A3G could completely inhibit (−) SSDNA synthesis (data not shown). This indicates that A3G inhibition of (−) SSDNA synthesis is dependent on the ratio of A3G:RNA.

It was also of interest to determine whether deaminase activity is required for the A3G inhibitory effect on

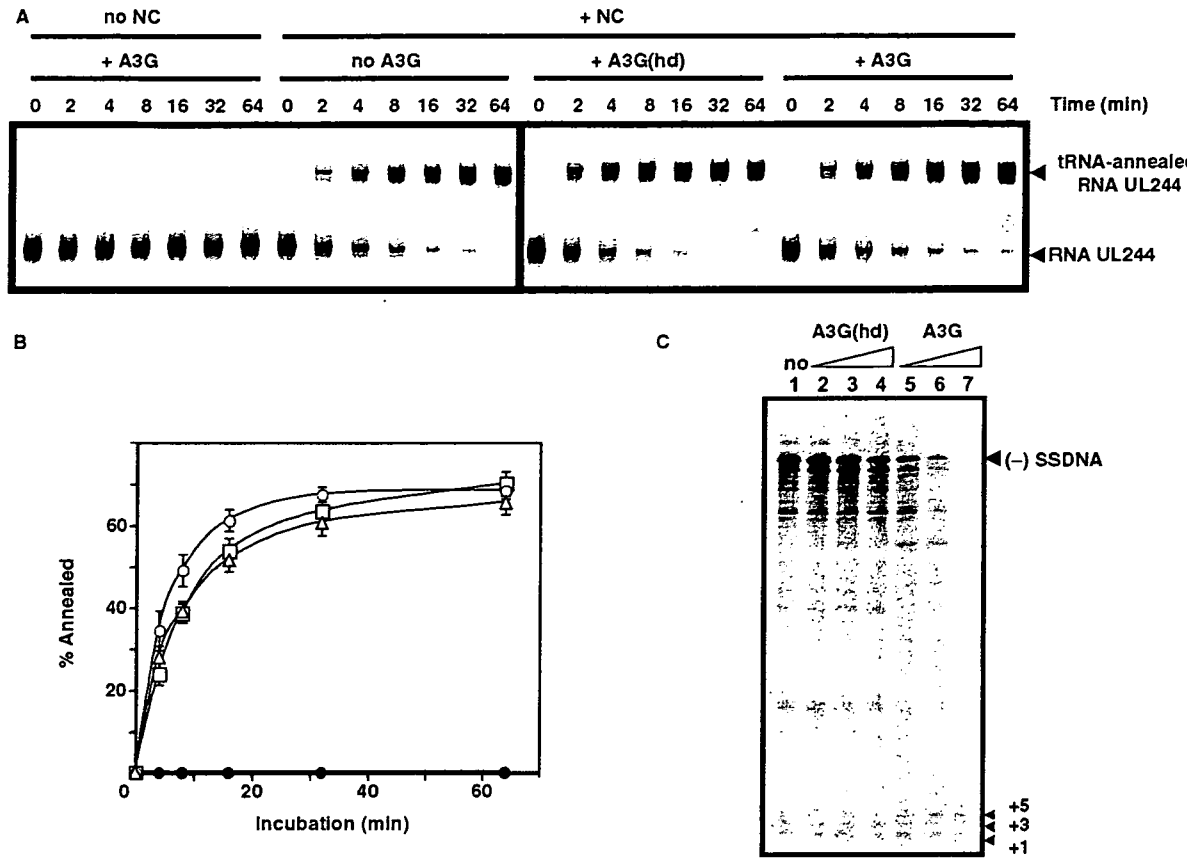

Figure 2. Effect of A3G on $tRNA_3^{Lys}$-primed (−) SSDNA synthesis. (A) Time course of $tRNA_3^{Lys}$ annealing to RNA UL244. Reactions were performed in the absence or presence of NC and A3G, as indicated by the headings at the top of the gel. The positions of the RNA UL244 template and the annealed RNA duplex are shown on the right. (B) The percentage of annealed product was calculated by dividing the amount of annealed RNA by the sum of annealed plus unannealed RNA, multiplied by 100. Symbols: no NC/no A3G (filled circles); + NC/no A3G (open squares); + NC/ + hdA3G (open circles); and + NC/ + A3G (open triangles). (C) A $tRNA_3^{Lys}$/RNA 244 complex was extended by HIV-1 RT in the absence (lane 1) or presence of hdA3G (lanes 2–4) or A3G (lanes 5–7). The positions of (−) SSDNA and initial pause products at bases + 1, + 3 and + 5 are shown on the right. A3G concentrations: lane 1, 0 nM; lanes 2 and 5, 20 nM; lanes 3 and 6, 40 nM; lanes 4 and 7, 80 nM.

(−) SSDNA synthesis. To address this question, we used purified deaminase-deficient A3G C291S protein (12) and then compared the effect of WT A3G or C291S on D18-primed (−) SSDNA synthesis. As shown in Figure 4, the rates and extents of (−) SSDNA synthesis in the presence of WT or mutant A3G were virtually the same, in accord with the observation that WT and C291S proteins have similar K_d values for binding to ss nucleic acids (12). The data of Figure 4 are significant and demonstrate that the inhibitory effect of A3G on (−) SSDNA synthesis is independent of A3G deaminase activity in our assay system.

Effect of A3G on minus-strand transfer reactions

Synthesis of a full-length minus-strand copy of the vRNA genome is achieved by transfer of (−) SSDNA to the 3′ end of vRNA ('acceptor RNA') followed by RT-catalyzed extension of the annealed DNA (Figure 1, step 3). This process (minus-strand transfer) is facilitated by base pairing of the complementary repeat regions at the 3′ ends of the nucleic acid substrates and is dependent on RNase H cleavage of vRNA sequences annealed to (−) SSDNA (43).

In Figure 5A, we show the time course of RNase H cleavage with the heat-annealed 59-bp TAR RNA/DNA hybrid, which was incubated with and without NC, in the absence or presence of A3G. Reactions containing A3G appeared to have slightly faster cleavage rates. However, the overall cleavage pattern was the same under all four conditions. These results indicated that A3G does not interfere with RNase H cleavage and is consistent with A3G's limited ability to bind to an RNA–DNA hybrid (6,12).

To assay the effect of A3G on minus-strand transfer, we first measured NC-mediated annealing using DNA 128 and acceptor RNA 148 (see schematic diagram in Figure 5C) in the absence or presence of A3G (Figure 5B). NC is required to transiently destabilize the complementary TAR RNA and DNA structures within the repeat region, before hybrid formation can occur (43).

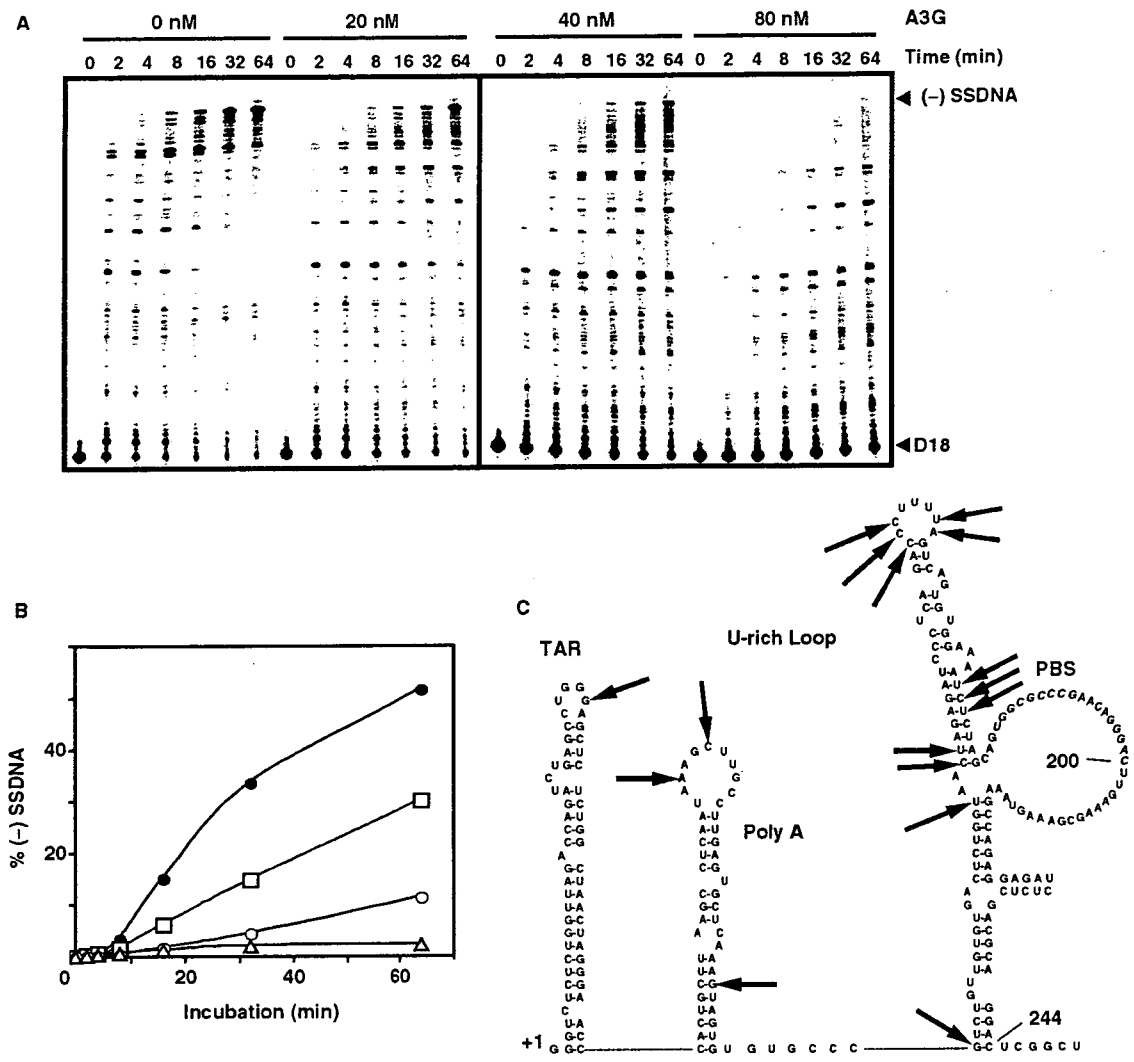

Figure 3. Effect of A3G on (−) SSDNA synthesis primed by D18. (A) Time course of (−) SSDNA synthesis in reactions containing ^{32}P-labeled D18 and RNA 244 in the presence of increasing concentrations of A3G. Positions of (−) SSDNA and D18 are shown on the right. (B) Graph of percent (−) SSDNA formed plotted versus incubation time. The percentage of (−) SSDNA product was calculated by dividing the amount of (−) SSDNA by the total amount of DNA, multiplied by 100. Symbols: 0 nM (filled circles); 20 nM (open squares); 40 nM (open circles); and 80 nM A3G (open triangles). (C) Mapping of pause sites on the RNA 244 template in A3G-containing reactions was based on the data shown in Figure S1. The arrows point to the pause sites.

Interestingly, A3G had only a minimal effect on annealing in the presence of NC. The rates were fairly similar with and without A3G and there was only a small reduction (11%) in the extent of the reaction when A3G was added. In a control reaction, we found that the extent of annealing minus NC, plus A3G was ~10% (data not shown), in accord with the value obtained in the absence of NC and A3G (63).

We also assayed minus-strand transfer with the complete system, which depends upon both annealing and RT-catalyzed elongation reactions (Figure 5C). The percent of total DNA present as the 182-nt strand transfer product (% Transfer Product) was quantified and plotted versus Time (Figure 5D). As we showed previously (49,64,65), NC significantly enhanced minus-strand transfer. However, when A3G was added, NC-mediated strand transfer was dramatically reduced (Figure 5D). Note that in the absence of NC, the amount of transfer product made was extremely small and little effect of A3G was observed.

Viewed collectively, the results of Figure 5 strongly suggest that A3G inhibited minus-strand transfer by blocking RT-catalyzed DNA elongation. In contrast, A3G did not significantly interfere with NC-facilitated annealing of (−) SSDNA to acceptor RNA. These findings parallel the results obtained for primer placement (Figure 2A and B) and tRNA-primed synthesis of (−) SSDNA (Figure 2C).

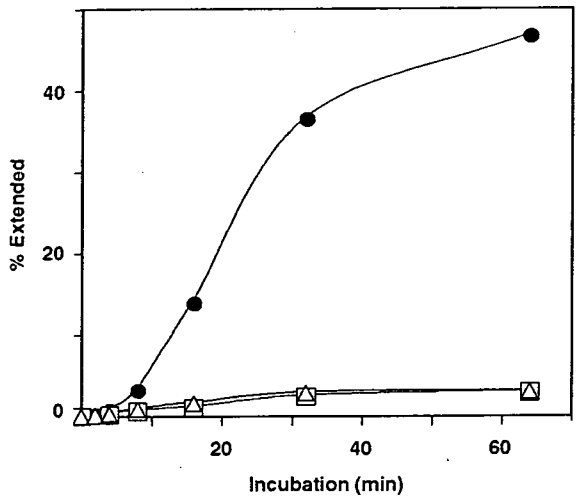

Figure 4. A3G inhibition of (−) SSDNA synthesis in the absence of deaminase activity. Symbols: no A3G (filled circles); WT A3G (80 nM) (open squares) and A3G C291S (80 nM) (open triangles).

Effect of A3G on (+) SSDNA synthesis and plus-strand transfer

While elongation of minus-strand DNA is being completed, the PPT RNA primer initiates synthesis of a short DNA termed (+) SSDNA (Figure 1, steps 4 and 5) (43). To determine whether A3G interferes with this step, we used a simple oligonucleotide assay that was previously developed in our laboratory (48,57). The 15-nt PPT was heat-annealed to a 35-nt minus-strand DNA template and the hybrid was then incubated with RT, which catalyzed the extension and subsequent removal of the PPT. The amount of 20-nt DNA product formed in reactions with and without A3G was quantified and plotted (Figure 6A).

The results demonstrated that A3G reduced both the rate and extent of (+) SSDNA synthesis by 2- to 3-fold. The effect of A3G on this reaction was lower than what we observed for (−) SSDNA synthesis (Figure 3A and B) or minus-strand transfer (Figure 5D). This is expected since long templates were used for those assays. By contrast, in the experiment shown in Figure 6A, only one or at most two molecules of A3G can bind to the available 20-nt ss region in the template (12,66). Nevertheless, it is clear from the data that A3G was also able to inhibit RNA-primed DNA-dependent DNA polymerization by RT.

The plus-strand transfer reaction, like minus-strand transfer, consists of two steps: (i) NC-mediated annealing of the complementary PBS sequences in (+) SSDNA and minus-strand acceptor DNA; and (ii) RT-catalyzed elongation of both the plus- and minus-strand DNAs to yield a double-stranded DNA product (Figure 1, steps 6–8) (43). In our assay, only the plus-strand ^{32}P-labeled 80-nt DNA is detected. In the absence of A3G, NC stimulated plus-strand transfer by 3-fold (Figure 6B), as reported previously (50). When A3G was added, reduction of synthesis was observed beginning at 10–15 min (e.g. at 15 min, by ~4-fold), whereas the extent of the reaction at 120 min was decreased by 2-fold. These results showed that A3G inhibited DNA-dependent DNA polymerization.

Taken together, the *in vitro* data demonstrate that A3G interfered with all of the elongation reactions catalyzed by RT. In contrast, A3G was shown to have virtually no inhibitory effect on NC-mediated annealing reactions.

Single molecule DNA stretching and FA-binding measurements

In an effort to understand these results, the nucleic acid binding properties of A3G, NC and RT were investigated using single molecule DNA stretching and FA.

When optical tweezers are used to stretch single DNA molecules by applying forces approaching 60 pN (Figure 7), a force-induced melting transition occurs, in which dsDNA is converted to ssDNA (59). In the absence of protein, this transition occurs over a very narrow force range due to the cooperative melting of DNA. Saturating levels of HIV-1 NC result in a significant increase in the width of the force-induced melting transition (46), which correlates with NC's relatively efficient chaperone activity. In addition, the reversibility of DNA stretch/relax curves in the presence of NC (i.e., DNA stretch curves show very little hysteresis), suggests that NC has a fast nucleic acid binding on/off rate and is therefore capable of rapidly switching between dsDNA and ssDNA bound states (60).

To probe the nucleic acid binding properties of A3G, we stretched single lambda DNA molecules in the presence of varying amounts of A3G (Figure 7A; data not shown) and characterized the transition width and hysteresis. The transition width increased from 3.7 ± 0.2 pN in the absence of protein to 18.3 ± 2.4 pN at protein saturation (~90 nM A3G and above). Examination of the stretching and relaxation curves showed that there was significant hysteresis (Figure 7A), which increased with A3G concentration, reaching a value of $\triangle G_{\text{hysteresis}} = 0.56 \pm 0.02$ kcal/mol per bp at 150 nM A3G, as compared to $\triangle G_{\text{hysteresis}} = 0.22 \pm 0.06$ kcal/mol per bp for saturated HIV-1 NC binding (Figure 7B) (60). The greater hysteresis in the presence of A3G reflects the inability of DNA to reanneal due to the presence of bound protein, which dissociates more slowly than the relaxation step time of ~1 s. In other experiments, RT was found not to have any measurable effect on lambda DNA stretching (Wang,F. and Williams,M.C., unpublished data).

The apparent binding affinities of HIV-1 NC, RT and human A3G to a 20-mer ssDNA oligonucleotide, 5′-FAM-JL587D, are given in Table 1 (also see Figure S2). HIV-1 NC binds to the 20-mer DNA with an approximately 3-fold greater affinity than human A3G. Both A3G and HIV-1 NC bind ssDNA with a significantly higher affinity (8- and 22-fold, respectively) than HIV-1 RT. These studies suggested that A3G should compete very effectively with RT for binding to ssDNA, but would not readily displace NC. Taken together with the stretching data, these results help to explain

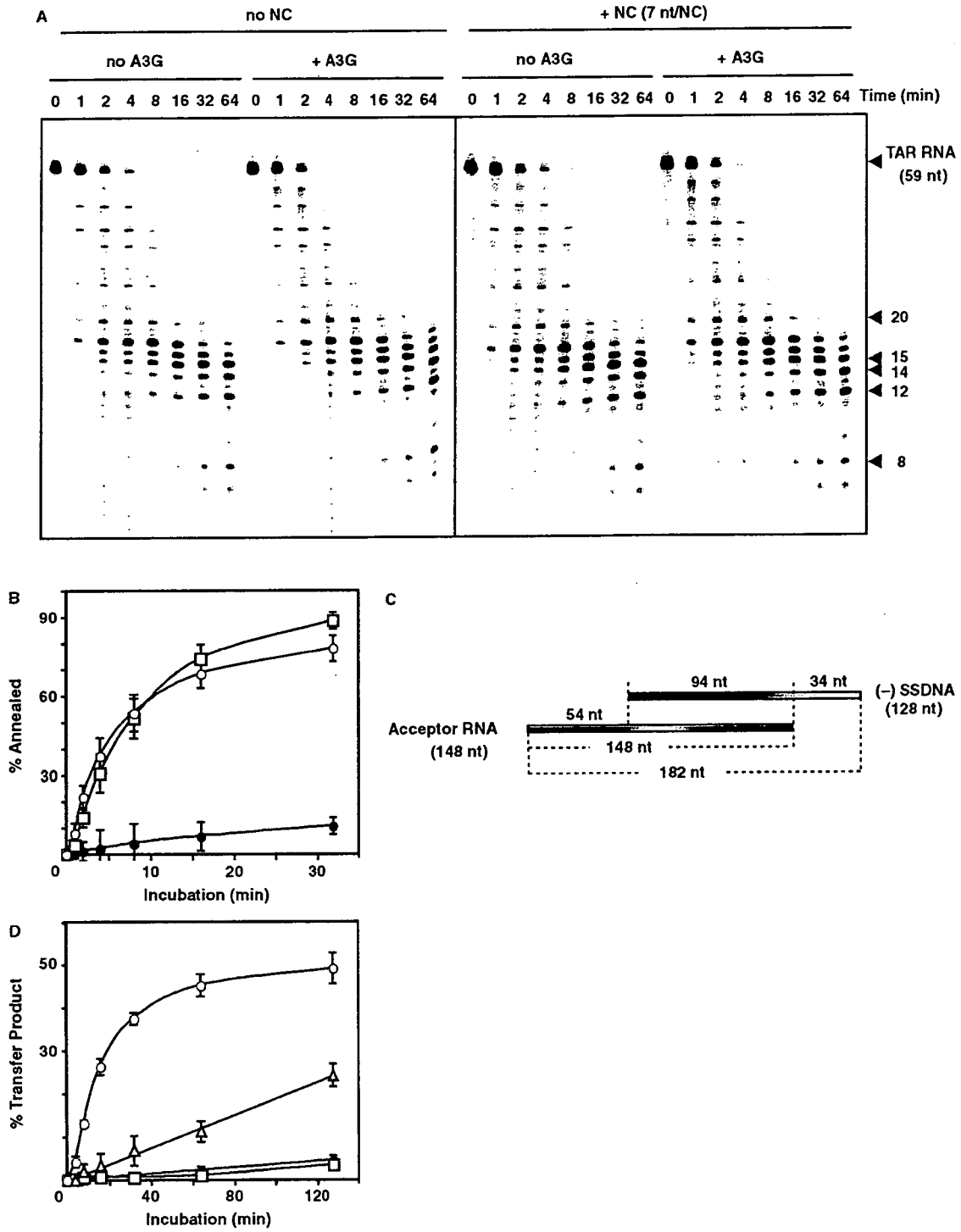

Figure 5. Effect of A3G on minus-strand transfer reactions. (A) Effect of A3G on the time course of RNase H cleavage in the absence or presence of NC. ^{32}P-labeled TAR RNA (0.1 pmol) and TAR DNA (0.2 pmol) were heat annealed and the hybrid was incubated at 37°C in reaction buffer (see above) with 0.4 pmol HIV-1 RT with or without NC (7 nt/NC, 0.1 μM), with or without A3G (80 nM). Samples were loaded on a 15% denaturing gel. Positions of the major cleavage products are indicated on the right. (B) Time course of annealing of ^{32}P-labeled DNA 128 to RNA 148 incubated in the absence or presence of A3G (80 nM) with or without NC (3.5 nt/NC, 0.4 μM). Symbols: no NC/+A3G (filled circles); +NC/no A3G (open squares); and +NC/+A3G (open circles). (C) Schematic diagram illustrating the minus-strand transfer assay system. The R homology is 94 nt; U5 and U3 are 34 and 54 nt, respectively. (D) Graph of percent transfer product plotted versus incubation time. To quantify the percentage of strand transfer, the amount of transfer product was divided by the total amount of DNA, multiplied by 100. Symbols: no NC/no A3G (filled circles); no NC/+A3G (open squares); +NC/no A3G (open circles); and +NC/+A3G (open triangles).

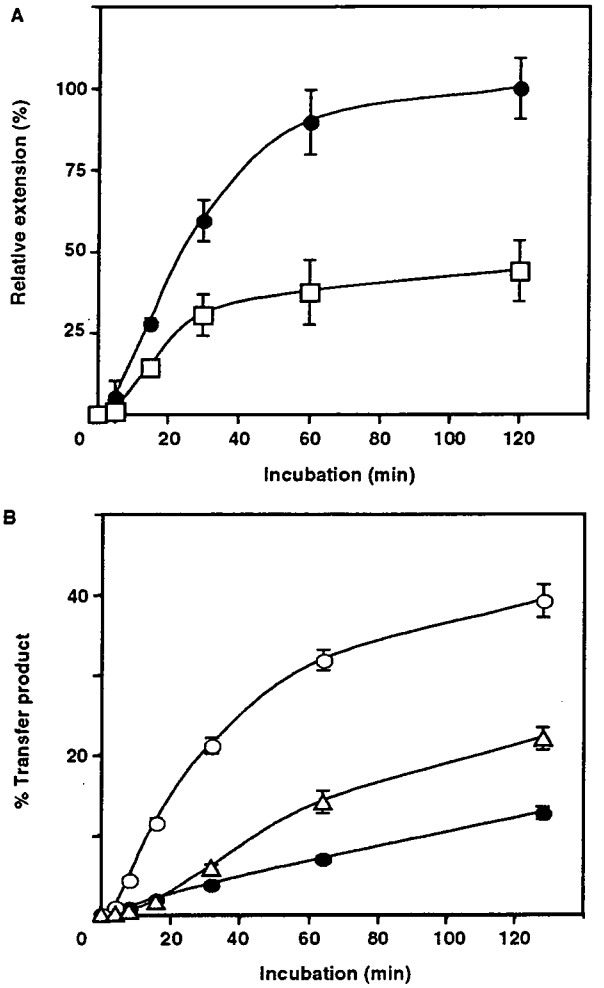

Figure 6. Effect of A3G on PPT initiation and plus-strand transfer. (A) Time course of PPT-primed plus-strand DNA synthesis. The 15-nt PPT RNA was heat-annealed to a 35-nt minus-strand DNA template and was then extended by HIV-1 RT. The 20-nt DNA product was internally labeled with [α-^{32}P]dCTP in the absence (filled circles) and presence (open squares) of A3G (80 nM). The amount of 20-nt DNA was plotted as Relative Extension (%) versus Time (min), where 100% represents the end point value for the 'no A3G' reaction. (B) Time course of plus-strand transfer. The percentage of 80-nt plus-strand DNA product was calculated as described in the legend to Figure 5D. Symbols: no NC/no A3G (filled circles); +NC/no A3G (open circles); and +NC/+A3G (open triangles).

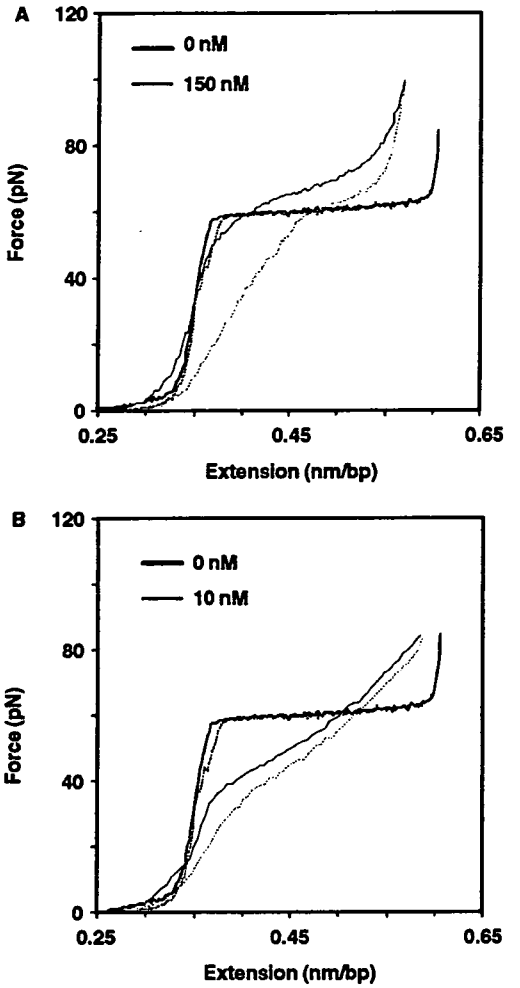

Figure 7. Examples of lambda DNA stretching (continuous) and relaxation (dashed) curves. (A) A3G. 0 nM (black); 150 nM (red). (B) NC. 0 nM (black); 10 nM (red). All stretching experiments were conducted at 20°C in 10 mM HEPES, pH 7.5 and 50 mM Na^+.

Table 1. Apparent binding affinities of HIV-1 NC, HIV-1 RT and A3G to 20-mer DNA oligonucleotide (5′-FAM-JL587D)

	K_d (nM)[a]
HIV-1 NC	84.1 ± 7.8
HIV-1 RT	1840 ± 390
A3G	238 ± 95

[a]K_d values were determined from three independent experiments. The error determinations represent the standard deviation.

why A3G inhibits RT-catalyzed elongation reactions, but fails to impact NC-mediated annealing.

DISCUSSION

Previous studies demonstrated that A3G inhibits reverse transcription during infection with Δ*vif* HIV-1 (28–31), with effects on synthesis of both early and late products (5,10,13,15,35–37). In the present study, for the first time, we show how A3G affects each individual step in reverse transcription (Figure 1), using a series of well-defined, reconstituted assay systems and highly purified A3G, RT and NC proteins. The results demonstrate that A3G inhibits elongation by HIV-1 RT directly, and not by blocking NC's nucleic acid chaperone activity (43). These findings are consistent with our previous result showing that NC and A3G do not compete for binding to RNA (12) and taken together, represent strong evidence that

at a physical and functional level, NC and A3G do not interfere with each other's activities.

More specifically, we report that A3G inhibits (−) SSDNA and (+) SSDNA synthesis, minus- and plus-strand DNA transfer, and elongation of minus- and plus-strand DNAs. Using a deaminase-deficient A3G mutant, we also show that (−) SSDNA synthesis was inhibited in the absence of A3G's enzymatic activity (Figure 4). Additionally, during (−) SSDNA synthesis in the presence of A3G, we find that RT pauses at unique sites, which map to bases in or near ss regions in the RNA template structure (Figure 3C; also see Figure S1), consistent with A3G's preference for binding to ss nucleic acids (6,12). Since a direct interaction between A3G and RT could not be detected in pull-down assays (data not shown), the results further suggest that A3G binding to the template physically blocks RT movement along the template. It should be noted that A3G has a more profound effect on DNA-primed DNA polymerase activity than the ss-binding protein T4 gene 32. Thus, in a primer extension assay with a DNA template, gene 32 protein inhibited minus-strand DNA synthesis at a concentration of 400 nM. In contrast, an A3G effect was already observed at a concentration of 12.5 nM and by 50 nM, the DNA product was no longer detectable (data not shown).

Systematic study of A3G inhibition of individual reverse transcription reactions is not amenable to investigation with more complex cell-based assays. However, PCR analysis has indicated that during infection, A3G inhibits synthesis of late DNA products to a greater extent than early products (15,35,37). Conceivably, successive inhibition at each step has a cumulative effect. Recently, Guo *et al.* (35) showed that reduction of early reverse transcripts in A3G-expressing cells infected with Δ*vif* virions is correlated with decreased tRNA priming *in vitro*. The authors suggested that an NC–A3G interaction might be inhibiting viral DNA synthesis. However, it was not determined whether A3G affected annealing and/or subsequent tRNA extension. In a new *in vitro* study, this group reports that in the presence of NC, A3G reduced $tRNA_3^{Lys}$ annealing by a little less than 2-fold (67). The reason for the difference between these results and our data showing that A3G does not inhibit NC-mediated primer placement (but has a strong effect on primer extension) (Figures 2 and 3) in all likelihood reflects significant differences in the experimental conditions for annealing with respect to the nt/NC ratio and the solution ionic strength.

Recently, it has been reported that A3G (15,37) and A3F (15) inhibit HIV-1 integration as well as reverse transcription. A3G and A3G C291S could each be specifically coimmunoprecipitated with NC and integrase (IN) present in HIV-1 Δ*vif* virions; coimmunoprecipitation of A3F with virion-associated IN could also be shown (15). Sequence analysis of 2-LTR circle junction clones from unintegrated DNA synthesized in the presence of A3G showed that in some cases, DNA at the U5 end had an additional 6 RNA bases derived from the 3′ terminus of $tRNA_3^{Lys}$. This suggests that A3G causes a defect in the tRNA removal step that limits plus-strand transfer and ultimately integration (37). Since we present definitive data showing that A3G does not inhibit RNase H cleavage of RNA in a preformed hybrid (Figure 5A), we suggest that the aberrant cleavage observed *in vivo* results from A3G binding to site(s) on the tRNA primer and/or the ssDNA template, thereby interfering with synthesis of plus-strand DNA (Figure 6A) and formation of a proper substrate for tRNA removal. Based on their results, Mbisa *et al.* (37) have made a similar proposal.

It was of interest to determine whether the A3G concentrations in the present study were within the physiological range. A recent report showed that only 7 (±4) molecules of A3G per virion are incorporated into *vif*-deficient HIV-1 produced from human PBMCs, indicating that only a few molecules of A3G are sufficient to inhibit HIV-1 replication (68). Interestingly, even the highest concentrations of A3G used in our experiments (up to 80 nM) are well below the estimated concentration of A3G in the virion (13 ± 8 μM). This value was obtained by assuming that the virus is a sphere of radius 60 nm (69).

Despite the high estimated concentration of A3G in the virus, the expected ratio of A3G:total nt of genomic RNA *in vivo* is much lower than the ratio that is typically used *in vitro*. However, RNA is highly folded and rarely ss (39). Indeed, the vast majority of vRNA is likely to be involved in secondary and tertiary interactions (70–72). Since A3G binds poorly to dsRNA (6,12), the effective ratio of A3G:ss nt *in vivo* is higher than predicted on the basis of total nt of RNA. Thus, the preferential binding of A3G to ssRNA (6,12) and the slow rate of A3G dissociation (Figure 7) could still result in A3G-induced inhibition of reverse transcription during infection.

The interpretation of the results presented here follows from our studies on the nucleic acid binding properties of NC, A3G and RT. Thus, the DNA stretching data in the presence of A3G show an increase in the force-induced melting transition width, suggesting that it is capable of binding to both ss and dsDNA. However, relative to NC, considerably higher concentrations of A3G are required to observe changes in the shape of the DNA stretching curve. Moreover, in sharp contrast to the small hysteresis observed with NC (Figure 7B), which decreases with increasing protein concentration (60), significant hysteresis is observed with A3G (Figure 7A). In this case, the amount of hysteresis increases when the protein concentration is elevated (data not shown). Similar behavior is observed with the ssDNA-binding protein T7 gene 2.5 (73), whose primary role in DNA replication is to stabilize ssDNA.

The DNA stretching results indicate that A3G binds preferentially to ssDNA and is unable to rapidly switch between binding to ssDNA and dsDNA. This finding can help to explain A3G's inhibition of reverse transcription, which requires rapid access of RT to the ssDNA or RNA template. Similarly, the fact that HIV-1 NC does not interfere with DNA synthesis is consistent with its ability to rapidly adjust to different binding states. The stretching data complement the FA–binding measurements, which show that the ssDNA binding order of the three proteins is NC>A3G>>RT (Table 1; Figure S2).